

Neutrophil extracellular traps melt Peyer's patches following stroke and myocardial infarction

Ali Tuz

Institute for Experimental Immunology and Imaging

Susmita Ghosh

Leibniz-Institut für Analytische Wissenschaften - ISAS-e.V., Dortmund, Germany

Markus Gallert

Institute for Experimental Immunology and Imaging

Dimitris Ttoouli

Faculty of Biology and Centre for Medical Biotechnology (ZMB), University of Duisburg Essen

Sai Sata

Leibniz-Institut für Analytische Wissenschaften - ISAS-e.V., Dortmund, Germany

Özgür Ulusoy

Institute for Experimental Immunology and Imaging

Andreas Kraus

Institute for Experimental Immunology and Imaging

Franziska Zwirnlein

Institute for Experimental Immunology and Imaging

Viola Kaygusuz

Institute for Experimental Immunology and Imaging

Vivian Lakovic

Institute for Experimental Immunology and Imaging

Alexander Beer

Institute for Experimental Immunology and Imaging

Altea Qefalia

Institute for Experimental Immunology and Imaging

Zülal Cibir

Institute for Experimental Immunology and Imaging

Medina Antler

Institute for Experimental Immunology and Imaging

Sebastian Korste

Department of Cardiology and Vascular Medicine

Lars Michel

University Hospital, University of Duisburg-Essen, DE-45147 Essen, Germany

Tienush Rassaf

University Hospital, University of Duisburg-Essen, DE-45147 Essen, Germany

Britta Kaltwasser

Department of Neurology, University Hospital, University of Duisburg-Essen, DE-45147 Essen, Germany

Hossam Abdelrahman

Institute for Experimental Immunology and Imaging

Ayan Mohamud-Yusuf

Department of Neurology, University Hospital, University of Duisburg-Essen, DE-45147 Essen, Germany

Chen Wang

Department of Neurology, University Hospital, University of Duisburg-Essen, DE-45147 Essen, Germany

<https://orcid.org/0000-0002-0213-9642>

Lars Haeusler

Institute for Experimental Immunology and Imaging

Smiths Lueong

German Cancer Research Center (DKFZ), Heidelberg, Germany

Martin Stenzel

Leibniz-Institut für Analytische Wissenschaften - ISAS-e.V., Dortmund, Germany <https://orcid.org/0000-0002-1378-2529>

Oliver Soehnlein

WWU Münster <https://orcid.org/0000-0002-7854-0694>

Benedikt Frank

Department of Neurology, University Hospital, University of Duisburg-Essen, DE-45147 Essen, Germany

Martin Köhrmann Köhrmann

University Hospital Essen, 45147 Essen, Germany.

Jens Siveke

German Cancer Consortium (DKTK) partner site Essen and Institute for Developmental Cancer Therapeutics (BIT), University Hospital Essen at the University Duisburg-Essen, Germany

<https://orcid.org/0000-0002-8772-4778>

Matthias Totzeck

University Hospital Essen, 45147 Essen, Germany.

Daniel Hoffmann

University of Duisburg-Essen <https://orcid.org/0000-0003-2973-7869>

Anika Grüneboom

Leibniz-Institut für Analytische Wissenschaften - ISAS-e.V., Dortmund, Germany

Nina Hagemann

Department of Neurology, University Hospital, University of Duisburg-Essen, DE-45147 Essen, Germany

Anja Hasenberg

Institute for Experimental Immunology and Imaging

Albert Sickmann

Jianxu Chen

Leibniz-Institut für Analytische Wissenschaften - ISAS - e.V. <https://orcid.org/0000-0002-8500-1357>

Dirk Hermann

Department of Neurology, University Hospital, University of Duisburg-Essen

Matthias Gunzer

University Duisburg-Essen

Vikramjeet Singh (✉ vikramjeet.singh@uni-due.de)

Institute for Experimental Immunology and Imaging

Article

Keywords: Stroke, myocardial infarction, immunosuppression, Peyer's patches, lymphocytes, neutrophil extracellular traps

Posted Date: June 13th, 2023

DOI: <https://doi.org/10.21203/rs.3.rs-3030780/v1>

License:   This work is licensed under a Creative Commons Attribution 4.0 International License.

[Read Full License](#)

Additional Declarations: There is **NO** Competing Interest.

Neutrophil extracellular traps melt Peyer's patches following stroke and myocardial infarction

Ali A Tuz¹, Susmita Ghosh², Markus Gallert¹, Dimitris Ttoouli³, Sai P Sata², Özgür Ulusoy¹, Andreas Kraus¹, Franziska Zwirnlein¹, Viola Kaygusuz¹, Vivian Lakovic¹, Alexander Beer¹, Altea Qefalia¹, Zülal Cibir¹, Medina Antler¹, Sebastian Korste⁴, Lars Michel⁴, Tienush Rassaf⁴, Britta Kaltwasser⁵, Hossam Abdelrahman¹, Ayan Mohamud Yusuf⁵, Chen Wang⁵, Lars Haeusler¹, Smiths Lueong⁶, Martin Stenzel², Oliver Soehnlein⁷, Benedikt Frank⁸, Martin Köhrmann⁸, Jens Siveke⁶, Matthias Totzeck⁴, Daniel Hoffmann³, Anika Grüneboom², Nina Hagemann⁵, Anja Hasenberg¹, Albert Sickmann², Jianxu Chen², Dirk M Hermann⁵, Matthias Gunzer^{1,2,*}, Vikramjeet Singh^{1,*}

¹ Institute for Experimental Immunology and Imaging, University Hospital, University of Duisburg-Essen, DE-45147 Essen, Germany

² Leibniz-Institut für Analytische Wissenschaften - ISAS-e.V., Dortmund, Germany

³ Bioinformatics and Computational Biophysics, Faculty of Biology and Centre for Medical Biotechnology (ZMB), University of Duisburg Essen, DE-45141 Essen, Germany

⁴ Department of Cardiology and Vascular Medicine, West German Heart and Vascular Center, University Hospital, University of Duisburg-Essen, DE-45147 Essen, Germany

⁵ Department of Neurology, University Hospital, University of Duisburg-Essen, DE-45147 Essen, Germany

⁶ Division of Solid Tumor Translational Oncology, German Cancer Consortium (DKTK, partner site Essen), German Cancer Research Center (DKFZ), Heidelberg, Germany

⁷ Institute for Experimental Pathology (ExPat), Center for Molecular Biology of Inflammation (ZMBE), Westfälische Wilhelms-Universität Münster, Münster, Germany.

⁸ Department of Neurology and Center for Translational Neuro- and Behavioral Sciences (C-TNBS), University Hospital Essen, 45147 Essen, Germany.

***Correspondence** to Vikramjeet Singh: vikramjeet.singh@uk-essen.de

and Matthias Gunzer: matthias.gunzer@uk-essen.de

Address

Institut für Experimentelle Immunologie und Bildgebung
Universität Duisburg-Essen
S05 V01 E24
Universitätsstr. 2
D-45141 Essen
Telefon: +49 201 / 183-6643
Telefax: +49 201 / 183-6642

Summary

Sterile tissue injury after stroke causes lymphocyte contraction in lymphoid tissues and may decrease circulating IgA-levels. Intestinal Peyer's patches (PP) harbor large numbers of IgA⁺ B cell precursors and plasma cells. Whether and how tissue injury triggers PP-B cell death, thereby mediating IgA-loss, is unknown. We found decreased circulating IgA levels in stroke and myocardial infarction patients. Experimental stroke and myocardial infarction in mice phenocopied the human situation. Decreased plasma and fecal IgA were accompanied by rapid and macroscopic shrinkage of PP caused by substantial losses of PP-resident IgA⁺ precursors and plasma cells in mice. Tissue injury induced neutrophil activation endowed with the release of toxic neutrophil extracellular traps (NETs). Antibody-mediated or genetically-induced neutrophil loss, digestion of NETs, or inhibition of their release by the Gasdermin D blockade completely prevented lymphocyte loss and PP shrinkage. We also identified NETs in the plasma of stroke and myocardial infarction patients. Hence, tissue injury induces systemic NET-release, which might be targeted to maintain immune homeostasis at mucosal barriers.

Keywords

Stroke, myocardial infarction, immunosuppression, Peyer's patches, lymphocytes, neutrophil extracellular traps.

Introduction

Stroke and myocardial infarction are life-threatening disorders with a few therapeutic options. Systemic bacterial infection is a frequent comorbidity and is associated with poor clinical outcomes. Ischemic tissue injury triggers exhaustion of over-activated immune cells and the resulting immunosuppression makes the mucosal barriers vulnerable to microbial invasion^{1, 2, 3}. Intestinal B cells are the major source of antibody-producing plasma cells and play a fundamental role in the protection of mucosal barriers. Peyer's patches (PP), central structures of gut-associated lymphoid tissues (GALT), contain substantial numbers of plasma cell precursors that later migrate to the lamina propria (LP) and secrete immunoglobulin (Ig) A antibodies⁴. Under homeostatic conditions, the generation of IgA-producing plasma cells occurs in the germinal centers of PP and requires complex interactions between B cells, antigen-presenting cells, and helper T cells⁵. The constant exposure of PP to commensal microflora or food antigens also induces tolerance in immune cells, thus inhibiting unwanted inflammation⁶ and autoimmunity⁷. Patients with ischemic stroke have decreased IgA levels and thus are at higher risk for bacterial infections⁸. Indeed, bacterial infections are a major reason for high mortality after stroke^{9, 10}. However, despite the important role of B cells in mucosal barrier defense and immune homeostasis, the effects of sterile tissue injury on intestinal B cells remain largely unexplored.

Here, we used experimental mouse models of ischemic stroke, myocardial infarction (MI) and blood samples from human stroke and MI patients to identify influences on intestinal B cell numbers and the amounts of circulating and secretory IgA antibodies. Using several molecular and imaging approaches, we found that the release of NETs triggers rapid and long-lasting loss of intestinal B cells which reduced the amounts of circulating IgA after ischemia-induced tissue injury. Inhibiting NET release from neutrophils by Gasdermin D blockade completely inhibited the loss of B cells after stroke.

Results

Tissue injury decreases IgA levels and intestinal lymphocytes

To determine the amounts of circulating IgA levels in stroke patients, we analyzed plasma samples by immunoassay and revealed a significant reduction in the circulating amounts of IgA within 72 h of hospital admission compared to healthy controls (Fig. 1a). Next, to determine the underlying mechanisms of stroke-induced IgA reduction, we employed a clinically relevant mouse model of ischemic stroke using transient (60 min) middle cerebral artery occlusion (tMCAO). Consistent with previous findings, the induction of brain ischemia resulted in reproducible brain infarcts and induced behavioral deficits at both one- and three-days post-injury (Extended Data Fig. 1a-c). Interestingly, like in human patients we identified a marked

reduction in the amounts of plasma and also fecal IgA after 24 h in stroke mice compared to sham controls (Fig. 1b, c). To elucidate whether intestinal Peyer's patches (PP), which harbor a large number of IgA-producing plasma cell precursors, were affected after stroke, we intended to investigate the tissue architecture and cellular composition of PP⁴. However, to our surprise, stroke reduced the size of PP so strongly that many of them were hardly visible by the bare eye (Fig. 1d). The smaller size of post-stroke PP also led to reduced numbers of harvested PP 72 h after stroke (Extended Data Fig. 1d). To further elucidate the extent of post-stroke PP shrinkage, we adapted our 3D light sheet fluorescence microscopy (LSFM) protocols of the optically cleared murine intestinal tract^{11,12} to perform a detailed volumetric analysis of PP (Extended Data Fig. 1e). The analysis confirmed a strong volume reduction ("melting") of PP in stroke mice 24 h and 72 h post-insult compared to sham controls (Extended Data Fig. 1f, g). However, a retrospective comparison between the volume of PP in sham and naïve mice did not show any differences, hence excluding any impact of the operation procedure on PP volume.

Previous studies have demonstrated that severe atrophy of spleen and thymus after stroke was the result of local lymphocyte apoptosis¹³. To analyze whether PP shrinkage was mediated via the loss of resident immune cells, we employed whole-mount immunostaining before LSFM analysis. Briefly, intestinal tissues with PP were stained with fluorescence-conjugated anti-CD19 and -CD3 antibodies and optically cleared before LSFM imaging (Fig. 1e, Extended Data Fig. 1e, and Video 1). The 3D reconstruction of imaging data showed a strong shrinkage of PP follicular structures containing CD19⁺ B cells 24 h after stroke (Extended Data Fig. 2a). For a thorough and consistent analysis of large numbers of samples, we developed a machine learning-based 3D volumetric image analysis (Extended Data Fig. 1h). The analysis of all LSFM images with this approach demonstrated that PP of stroke mice exhibited significantly smaller volumes of CD19⁺ B cell follicles in the jejunum and ileum compared to similar regions in sham controls (Fig. 1f and Video 2). In addition, stroke also caused a significant reduction of CD3⁺ T cell zone volumes in PP isolated from the ileum (Extended Data Fig. 2b).

To test whether these findings were specific to stroke or rather a global response to large-scale tissue injury, we studied circulating levels of IgA in patients with myocardial infarction (MI) within 96 h of hospital admission. Interestingly, similar to the stroke patients, also MI patients presented reduced amounts of plasma IgA (Fig. 1g). To study if the reduced plasma IgA amounts in MI patients were also related to the shrinkage of PP we utilized a murine model of myocardial ischemia-reperfusion injury^{14,15}. Interestingly, also the induction of myocardial infarction in mice caused the shrinkage of PP B cell follicles in the intestinal jejunum and ileum

and T cell zone volumes in the jejunum as compared to sham controls (Fig. 1h and Extended Data Fig. 2d).

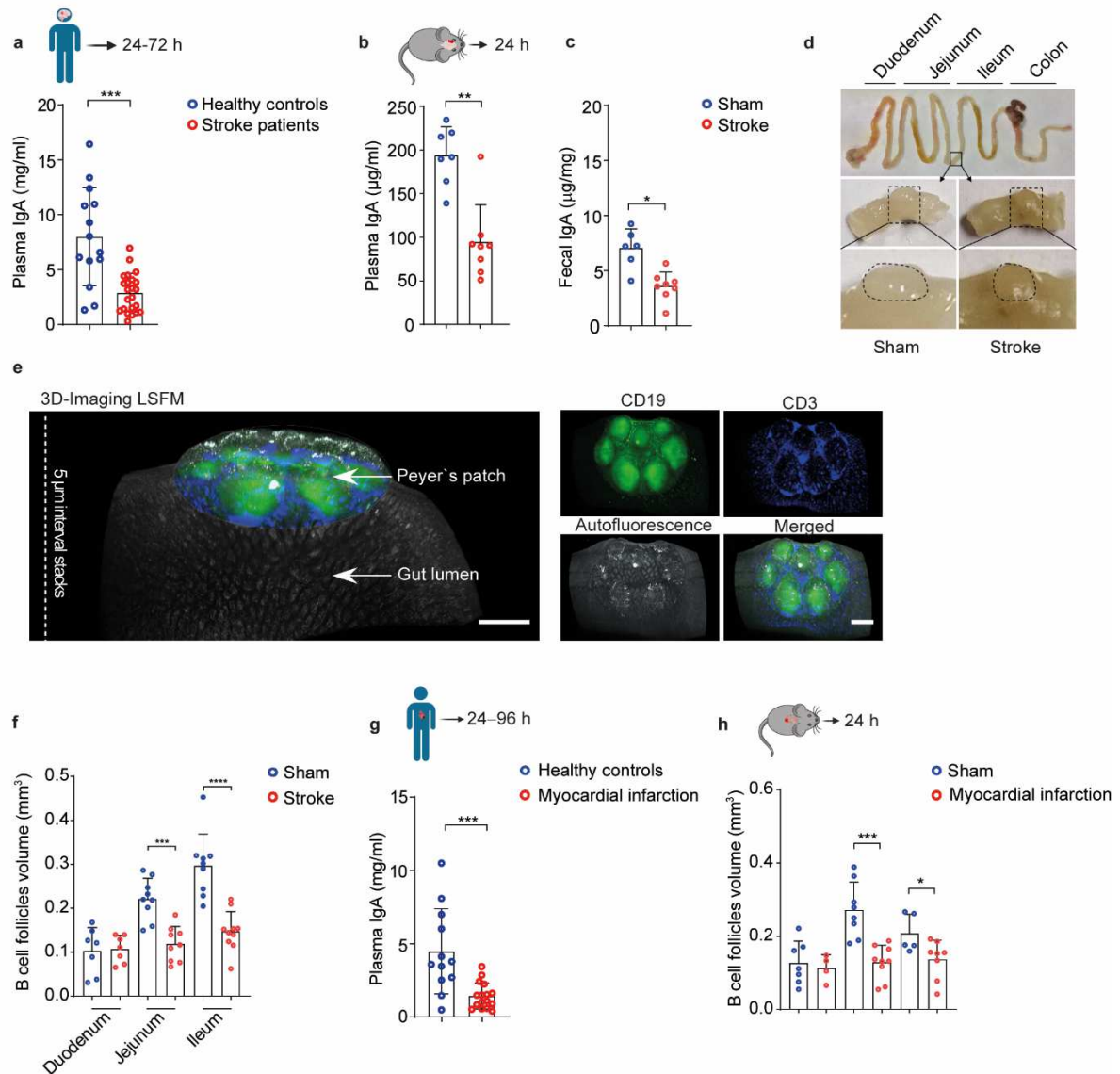


Fig. 1. Ischemic stroke and myocardial infarction reduce plasma IgA levels and B cell follicles volume in Peyer's patches. **a**, Stroke patients showed reduced amounts of plasma IgA compared to healthy subjects (n=12–23 per group). **b**, **c** Stroke significantly reduced plasma and fecal IgA levels in mice compared to sham controls (n=6–8 per group). **d**, Macroscopic overview of the mouse gastrointestinal tract with the demarcation of PP one day after sham surgery or stroke. **e**, Fluorescence images after 3D reconstruction of stained PP showing the position of PP in the small intestine that were whole-mount stained with anti-CD19 (green) and anti-CD3 (blue) fluorescent antibodies before LSFM (left), scale bar= 500 µm. Fluorescence single-channel images are shown (right). **f**, Deep learning-based automated analysis of B cell follicle volume in PP from duodenum, jejunum and ileum one day after stroke or sham controls (n=7–11 PP per intestinal segment). **g**, The concentrations of plasma IgA were measured in myocardial infarction patients and healthy controls by ELISA (n=12–16 per group). **h**, Deep learning-based quantification of B cell follicle volume in PP of the duodenum, jejunum and ileum one day after sham or myocardial infarction (n=4–9 PP per intestinal segment). Data are mean ±s.d., statistical analyses were performed by two-tailed Mann-Whitney U test, *p<0.05, **p<0.01, ***p<0.001. All mice data are combined from at least three independent experiments. tMCAO= transient middle cerebral artery occlusion.

Of note, a specific absence of B cells in $J_{HT}^{-/-}$ mice¹⁶ or their depletion using antiCD20 antibodies greatly reduced the size of PP compared to controls, thus highlighting a major contribution of B cells in maintaining their tissue integrity (Extended Data Fig. 2e). Collectively, these results showed a strong effect of sterile tissue injury on the rapid and massive loss of PP-resident B and T cells without affecting the overall numbers of detectable individual B cell follicles in the affected PP (Extended Data Fig. 2f).

Stroke affects the survival of intestinal immature and mature plasma cells

To further quantify the influence of stroke on specific lymphocytes, we investigated their total numbers in PP, small intestine lamina propria (SI LP), mesenteric lymph nodes (mLN), bone marrow (BM) and blood using flow cytometry (Extended Data Fig. 3a,b). Our results showed that the majority of immune cells in PP were CD19⁺ B (78 ±10%) and CD3⁺ T (18 ±5%) cells with a small fraction of CD11b⁺ Ly6G⁻ monocytes (<2%) and Ly6G⁺ CD11b⁺ neutrophils (<1%) (Extended Data Fig. 3c). However, SI LP showed reverse frequencies of CD19⁺ B (18 ±4%) and CD3⁺ T (61 ±4%) cells (Extended Data Fig. 3d). As expected, stroke strongly reduced the total numbers of CD19⁺ B cells and CD3⁺ T cells in PP after 24 h (Fig. 2a). The absence of lymphocyte loss in sham mice compared to naïve controls validated the contribution of stroke on the massive loss of B and T cells in PP. In keeping with our previous data^{17, 18}, stroke also strongly decreased the numbers of B and T cells in spleen compared to controls (Extended Data Fig. 4a). However, the lymphocyte numbers in mesenteric lymph nodes, bone marrow and blood were not significantly reduced (Extended Data Fig. 4b-d).

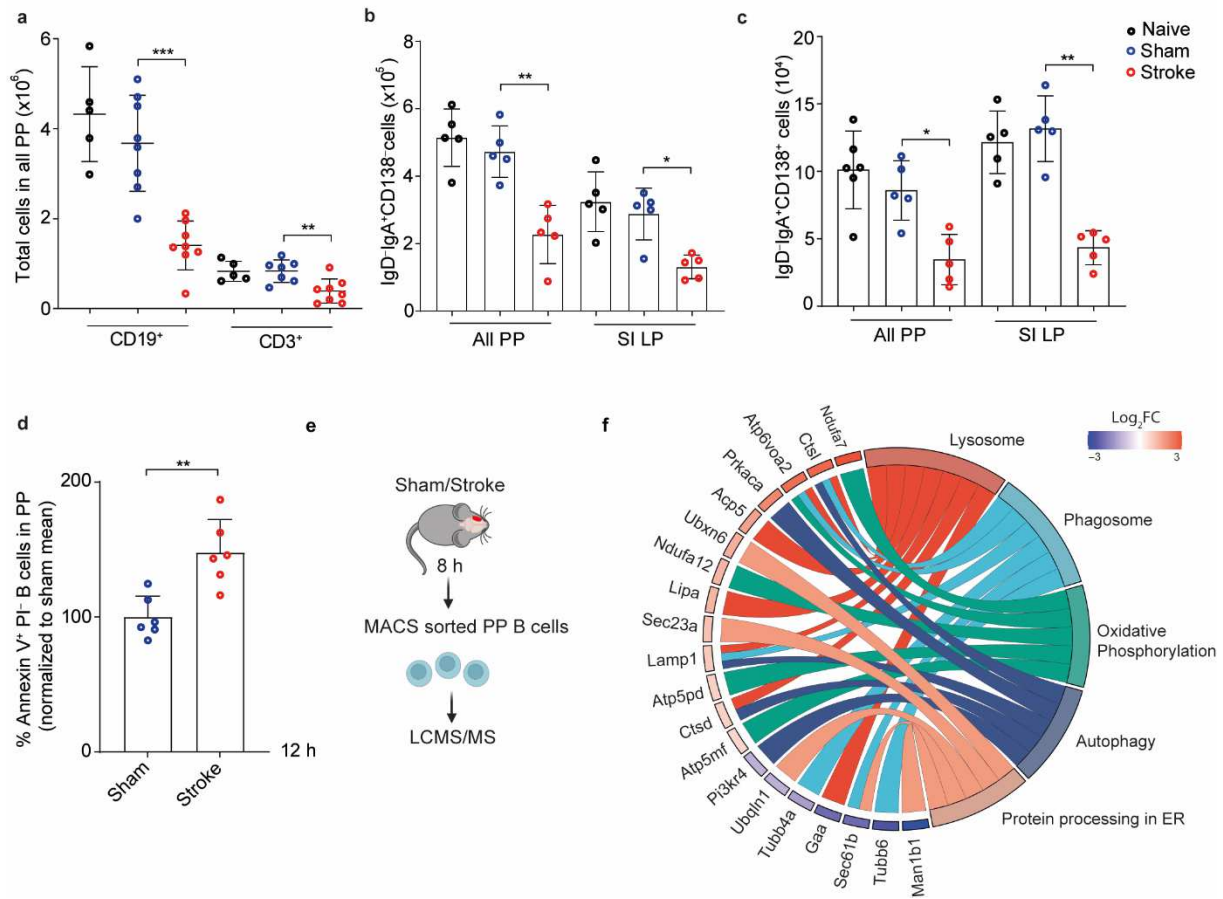


Fig. 2. Stroke induces B cell loss in PP via activation of cell death pathways. **a**, Flow cytometry–based quantification of the number of CD19⁺ B cells and CD3⁺ T cells in all intestinal PP 24 h after sham surgery or stroke and unoperated naïve mice (n=5–8 per group). **b**, Quantification of IgA⁺ IgD⁻ CD138⁻ plasma cell precursors in all PP and SI LP after 24 h of sham surgery or stroke and naïve mice (n=5 per group). **c**, Quantification of IgA⁺ IgD⁻ CD138⁺ plasma cells in all PP and SI LP (n=5 per group). **d**, Single–cell suspensions from PP of sham and stroke mice were prepared 12 h after the operation and apoptotic cells were quantified by staining with Annexin V and PI followed by flow cytometry analysis (n=6 per group). **e**, After sham–operation or stroke, B cells from PP were enriched using MACS and analyzed by mass spectrometry (n=3 per group). **f**, Gene ontology Chord diagram of the functional enrichment analysis. Genes are ranked based on Log₂FC value (high to low). Each Chord connects the gene with its associated pathway. Data are mean ±s.d., statistical analyses were performed by two–tailed Mann–Whitney U test, *p<0.05, **p<0.01, ***p<0.001. All data are combined from at least three independent experiments. PP=Peyer’s patches, SI LP= small intestine lamina propria.

Further flow cytometry analyses revealed a reduction in the numbers of IgD⁻ IgA⁺ CD138⁻ plasma cell precursors in total PP and SI LP in stroke mice compared to sham controls^{19, 20} (Fig. 2b). In PP, B cells are primed by signals from the intestinal microflora and other immune cells to produce IgA⁺ secreting plasma cells^{21, 22}. Our data showed that stroke significantly decreased the number of IgD⁻ IgA⁺ CD138⁺ plasma cells in PP and SI LP (Fig. 2c). Next, we opted for different *in vivo* experiments to delineate the mechanisms of B cell loss in PP after stroke. Interestingly, the induction of stroke significantly increased the percentage of

Annexin V⁺ PI⁻ apoptotic B cells within 12 h compared to sham controls (Fig. 2d). To preclude an active egress of B cells from PP after stroke, we consistently analyzed other lymphoid tissues 12 h after surgery. Our data did not show any increase in the percentages of B cells in blood, mLN and SI LP compared to sham controls (Extended Data Fig. 4e).

To study the impact of stroke on the molecular makeup of PP B cells, we performed mass spectrometry-based proteomics analyses after 8 h (Fig. 2e). With a label-free quantitative proteomics approach, 3,997 proteins in total were quantified from B cells of both conditions (n=3 for each condition) with 1% false discovery rate [FDR]. The statistical analysis of normalized and missing value imputed data resulted in a list of 185 differentially expressed proteins that passed the t-test (adjusted p-value 0.05) with a log₂(fold change) ≥ 0.58. Of those, 99 proteins were upregulated and 86 proteins were downregulated in B cells isolated from stroke compared to sham-treated animals. Interestingly, functional enrichment analysis of differentially expressed proteins showed dysregulation of pathways associated with lysosome and phagosome function, autophagy, oxidative phosphorylation and the endoplasmic reticulum (Fig. 2f). Autophagy-associated proteins like Catsl²³ and Lamp1²⁴ were significantly upregulated in B cells from stroke mice. Moreover, the upregulated proteins Ndufa7²⁵ and Atp6voa2²⁶ are involved in oxidative phosphorylation. This can be a response to DNA damage and cell stress since Atp6voa2 is specifically known to be an essential factor for autophagy²⁶ and Ndufa7 is associated with ROS detoxification^{27, 28}. Overall, these data indicate that stroke may trigger specific B cell stress pathways and possibly excessive autophagy-mediated cell death²⁹.

Long-term metabolic dysfunction in B cells after stroke

We next aimed to investigate the duration of B cell loss from PP after stroke which is therapeutically relevant to identify a potential need to treat prolonged intestinal immune imbalance. Our data showed a drastic decrease in B cell numbers after 12 h in stroke mice compared to sham controls (Fig. 3a). Interestingly, B cell numbers after stroke did not recover until seven days which was the endpoint of this experiment. To reveal the underlying mechanisms of this long-term loss of cells, we purified PP B cells from mice 18 h after sham-operation or stroke and analyzed transcriptomic changes by bulk RNA sequencing and bioinformatic analysis. Interestingly, a principal component analysis (PCA) showed that the transcriptomes of B cells clustered separately in stroke mice and sham controls (PC1, at 51%) (Fig. 3b). Moreover, 447 genes were upregulated and 198 genes were downregulated (absolute fold change ≥2 and adjusted p-value <0.05) in B cells following stroke compared to sham controls (Fig. 3c). As expected, cell death genes (Bmf, Pdcd4, Bbc3 and Znr1)^{30, 31} were enriched while cell function genes (Egr3, Ankrd37, Rasgef1b) and cell metabolic genes (Fuca-

1, Smpd3, Acsl3, Ldlr and Entpd5) were reduced in B cells of stroke compared to sham control mice (Fig. 3c).

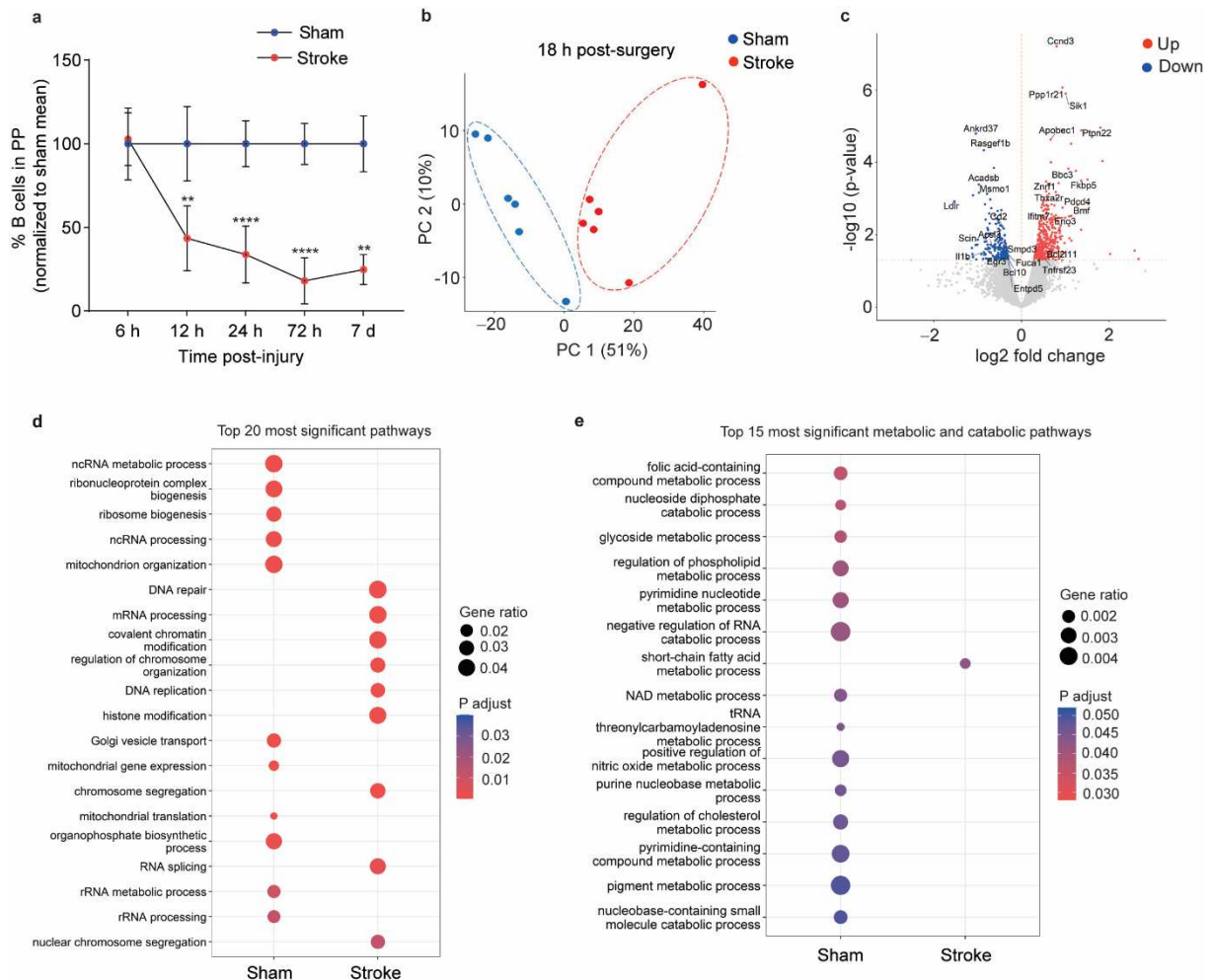


Fig. 3. Stroke downregulates cellular and metabolic functions of B cells in PP. **a**, Kinetics of B cell loss in PP of stroke mice compared to sham controls. Data are presented as a percentage decrease in B cell numbers in stroke mice normalized to sham controls for each time point (n=6–9 per group and time-point). **b**, Principal component analysis (PCA) of RNA-seq data of CD19⁺ B cells in PP from mice exposed to sham surgery or stroke (n=6 mice per group). **c**, Volcano plot showing statistically significant differentially expressed genes in PP B cells of stroke mice compared to sham. Red dots indicate upregulated genes and blue dots indicate downregulated genes. **d**, Gene set enrichment analysis (GSEA) of RNA-seq showing enriched cell function pathways in sham-operated and stroke mice. **e**, GSEA showing enriched metabolic/catabolic pathways in PP B cells of stroke and sham-operated mice. The dot size indicates the calculated gene ratio and the dot color indicates the adjusted p-value representing the enrichment score as described in the methods. Note that B cells from stroke mice are metabolically shut-down. Data represent mean \pm s.d., two-tailed Mann-Whitney U test: **p<0.01, ****p<0.0001. All data is combined from at least two-three independent experiments, n=6 mice per group. PP=Peyer's patches, Up=upregulated genes, Down= downregulated genes.

B cells from stroke mice expressed higher levels of the Myc target gene cyclin Ccnd3 and B cell lymphoma Bcl2, a key regulator of clonal expansion³² and survival³³, respectively. In addition, stroke enriched the expression of Sik1 and Ptpn22 in B cells which are involved in cell differentiation and B cell receptor signaling^{34, 35}. These findings indicated that in parallel to the activation of pro-apoptotic genes, some B cell subsets may have upregulated survival genes after stroke, potentially as compensatory mechanisms. Furthermore, we performed gene set enrichment analyses to identify cellular processes that were affected in B cells after stroke. The differentially expressed genes enriched in B cells of stroke mice were related to chromatin and histone remodeling, DNA replication and repair (Fig. 3d). Notably, the pathways responsible for mitochondrial organization and function, ribosome biogenesis, and Golgi vesicle transport were decreased in B cells of stroke mice, suggesting severe metabolic disturbances in these cells. Further analyses showed a complete downregulation of pathways related to several metabolic and catabolic processes in B cells after stroke compared to sham controls (Fig. 3e).

Based on our previous experience with the tMCAO mouse model, animals consume less food after stroke compared to sham controls and this may additionally impact the cell metabolism and B cell numbers in PP. To exclude that suboptimal food supply after stroke compared to sham was responsible for B cell death and PP shrinkage, stroke and sham mice were gavaged with liquid food and sacrificed 24 h post-ischemia-reperfusion injury (Extended Data Fig. 4f). The analysis showed, that stroke still reduced the numbers of B and T cells in PP compared to sham controls, thus excluding a potential role of reduced food intake after surgery for PP melting (Extended Data Fig. 4g). Collectively, these data identified several key transcriptional and molecular changes in PP B cells after distant tissue injury and highlighted severe long-term immune disturbances in the intestinal mucosal tissues after a stroke event.

Circulating DNA triggers lymphocyte reduction in intestinal tissues

While B cell death in PP after tissue injury was a robust finding, the broad underlying mechanisms remained unsolved. To elucidate this phenomenon, we focused on our earlier concept of soluble DNA as a death-mediator released after tissue injury¹⁷. In line with our previous findings, we found an early (6 h) increase in circulating DNA (ciDNA) in stroke mice compared to controls (Fig. 4a). The amounts ciDNA were decreased 24 h after stroke but still significantly higher than in sham controls. Similarly, also myocardial infarction increased the levels of ciDNA at 6 h which, however, returned to sham levels at 24 h (Extended Data Fig. 4h). To test a potential causative role of ciDNA for B cell loss in PP, we treated the mice with recombinant DNase-I immediately after stroke. Interestingly, the degradation of ciDNA significantly inhibited the loss of PP B cells (Fig. 4b) and T cells (Fig. 4c). Moreover, DNase-I treatment did not affect brain infarct volumes (Fig. 4d) at this early time point of 24 h post-

insult, thus indicating a direct blockage of B cell loss with DNase-I and ciDNA acting as a soluble mediator released after stroke.

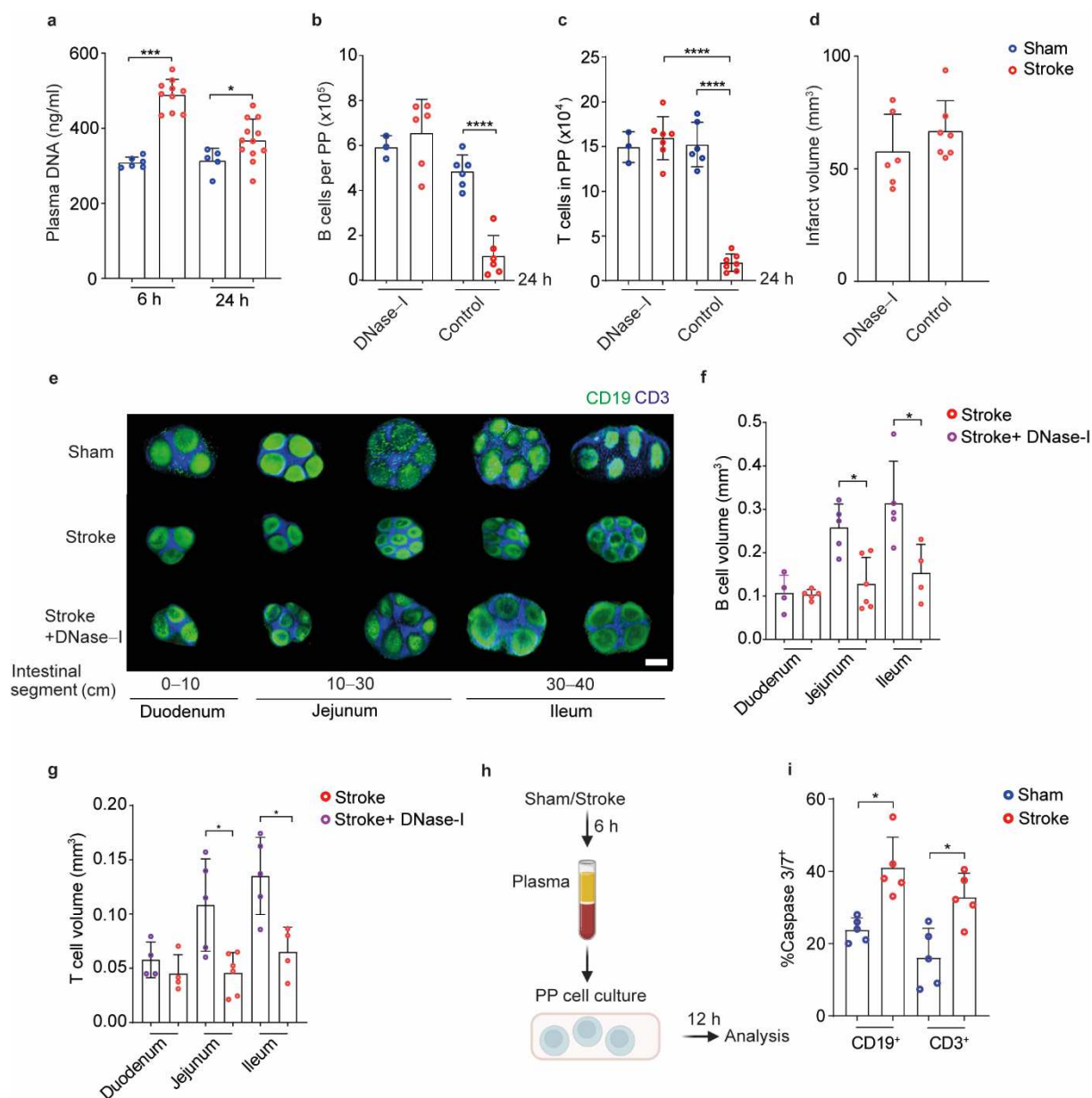


Fig. 4. Stroke increases ciDNA and promotes lymphocyte loss in PP. **a**, Quantification of plasma DNA 6 h and 24 h after sham surgery or stroke using Qubit assays ($n=5-12$ per group). **b**, Numbers of B cells in PP 24 h after sham surgery or stroke in DNase-I and vehicle-treated mice analyzed by flow cytometry. **c**, Numbers of T cells in PP 24 h after sham-operation or stroke in DNase-I and vehicle-treated mice. **d**, Brain infarct volumes in DNase-I treated and untreated mice at 24 h ($n=6-7$ per group). **e**, 3D reconstruction LSFM images of CD19⁺ B cells and CD3⁺ T cells in PP after sham, stroke and stroke + DNase-I treated mice, scale bar=500 μm . **f**, Quantification of CD19⁺ B cell follicle volume and **g**, T cell zone volume in duodenum, jejunum and ileum 24 h after stroke or stroke + DNase-I treatment ($n=4-6$ PP per intestinal segment). **h**, Schematic of the experimental paradigm. Mice undergo stroke or sham-operation and sacrificed after 6 h to collect blood plasma. Cell cultures from PP were prepared and treated with the plasma of sham or stroke mice for 12 h. The quantification of caspase-3/7-expressing cells was performed by flow cytometry. **i**, The percentages of caspase-3/7⁺ B and T cells in PP cell cultures incubated with

plasma of stroke or sham-operated mice. Data are mean \pm s.d., * $p < 0.05$, *** $p < 0.001$, **** $p < 0.0001$, Shapiro-Wilk normality, and ordinary one-way ANOVA with Bonferroni's multiple comparisons tests and for comparisons between two groups two-tailed Mann-Whitney U test. PP=Peyer's patches.

Since ciDNA degradation with DNase-I prevented B cell loss in PP, we investigated whether this treatment also preserved the mesoscopic structure of intestinal PP in stroke mice. LSFM analysis indeed confirmed that DNase-I treatment after stroke completely preserved PP structural integrity ($p < 0.05$) (Fig. 4e), and the volume of B and T cell compartments in the affected intestinal segments (Fig. 4f, g). To prove the contribution of plasma components as a cause of lymphocyte death, we used plasma of sham- or stroke mice (6 h post-injury) for further *ex vivo* analysis and incubated it with PP cell cultures (Fig. 4h). The treatment of PP cells with plasma of stroke mice significantly increased the percentage of caspase-3/7⁺ B and T cells, supporting the concept of circulating mediators directly inducing cell death (Fig. 4i).

Neutrophils are the major contributor to ciDNA after stroke

Next, we explored the potential sources of the additional amounts of ciDNA after stroke. Activated neutrophils are the first intruders to injured inflammatory tissues and respond via the release of neutrophil extracellular traps (NETs)³⁶.

To find out, whether circulating neutrophils in stroke mice were activated, we characterized their molecular makeup 6 h after sham surgery or stroke using mass spectrometry (Fig. 5a). The comparative and label-free quantitative proteomic analysis yielded 1,757 proteins with ≥ 2 unique peptides and 1% FDR. A sample-wise comparison showed a Pearson correlation coefficient of ≥ 0.93 , indicating high technical reproducibility (Extended Data Fig. 5a). Interestingly, the PCA showed a clear separation between circulating neutrophils of sham and stroke mice (Fig. 5b) based on their proteome. Of the 89 significantly altered proteins (adjusted p -value < 0.05 and fold change ≥ 1.5), 32 were up- and 57 proteins were down-regulated in neutrophils of stroke mice compared to sham controls (Fig. 5c). Remarkably, proteins associated with neutrophil degranulation (Lamp1, S100a8, CD47) and neutrophil activation (Il1r2, Stat3) were upregulated in stroke mice. In addition, the increased abundance of apoptotic proteins (Aifm1, Casp3) and the deficiency of cell function proteins (Pla2g7, Spta1, Sptb, Ipo5, Bsg, Gp1ba, Ptk2b) in stroke mice indicated the activation of cell-death pathways in neutrophils that have been observed in association with chromatinolysis³⁷ and NETosis^{38, 39}.

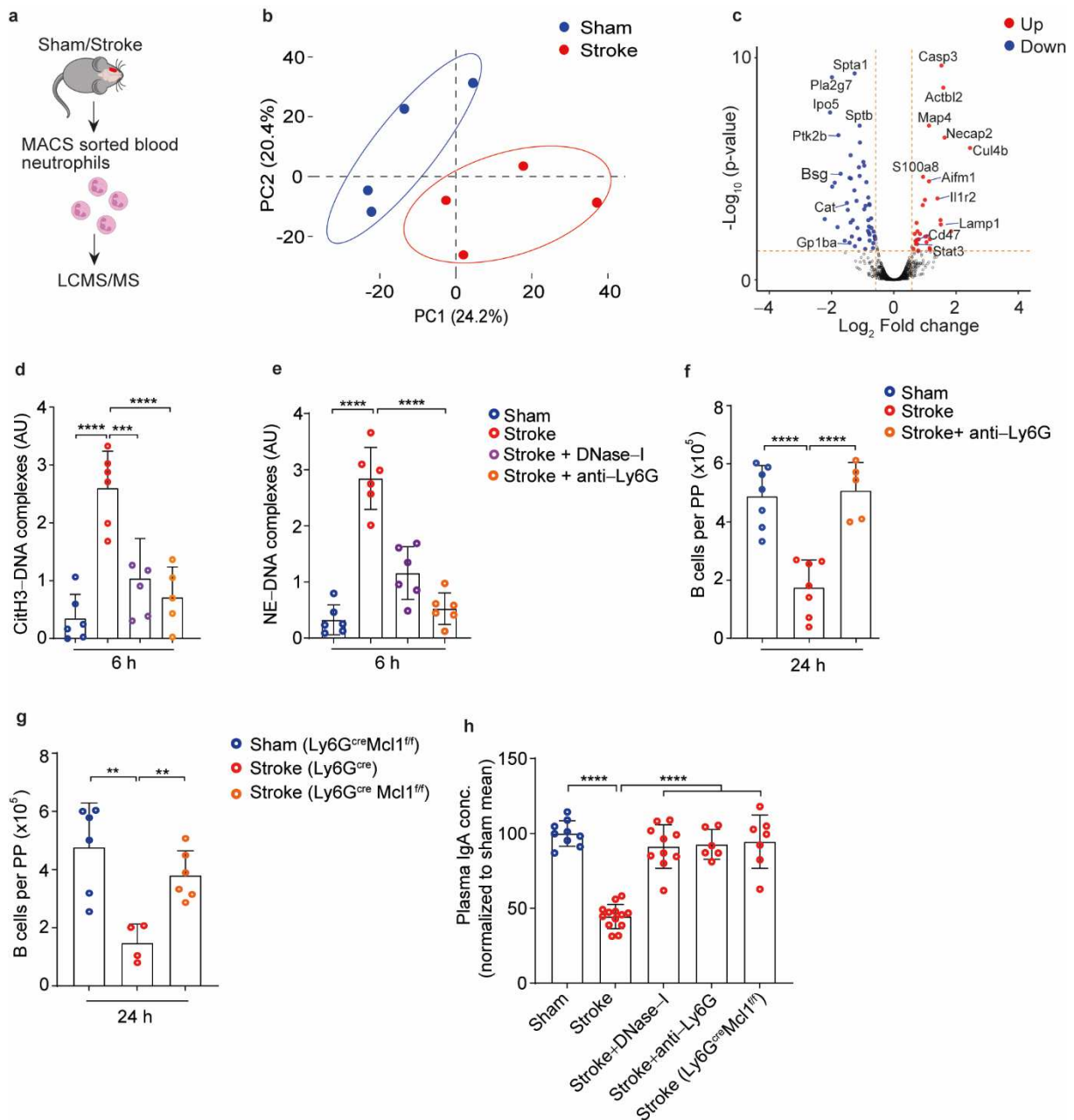


Fig. 5. Stroke activates circulating neutrophils to release cytotoxic NETs which induce B cell loss. **a**, Schematic of the experimental paradigm for neutrophil mass-spectrometry and proteomics analysis. Blood neutrophils were isolated 6 h after sham surgery or stroke to perform LCMS/MS analysis. **b**, PCA of neutrophil proteomics after sham or stroke (n=4 mice per group). **c**, Volcano plot comparing the normalized protein abundance in blood neutrophils of stroke mice vs sham-operated mice. Red dots indicate significantly upregulated proteins and blue dots indicate significantly downregulated proteins. **d**, Relative plasma levels of citH3-DNA or **e**, NE-DNA complexes after sham + isotype antibody, stroke + isotype antibody, stroke + DNase-I treatment or stroke + anti-Ly6G antibody treatment (n=5-6 per group). **f**, Numbers of CD19⁺ B cells in intestinal PP in sham-operated + isotype antibody, stroke + isotype antibody and stroke + anti-Ly6G antibody-treated mice. **g**, Numbers of CD19⁺ B cells in PP in sham-operated Ly6G^{cre}Mcl1^{fl/fl} mice, stroke Ly6G^{cre} and Ly6G^{cre} Mcl1^{fl/fl} mice (n=4-6 per group). **h**, Quantification of plasma IgA amounts sham, stroke, stroke + DNase-I treatment, stroke + anti-Ly6G antibody treatment or stroke Ly6G^{cre} Mcl1^{fl/fl} mice (n=6-13 per group). Data represent mean \pm s.d., **p<0.01, ***p<0.001,

**** $p < 0.0001$, Shapiro–Wilk normality, and ordinary one–way ANOVA with Bonferroni’s multiple comparisons tests. PP=Peyer’s patches, CitH3=citrullinated Histone-3, NE=neutrophil elastase.

To determine whether NETs were indeed released into the circulation after stroke, we measured the plasma content of citrullinated histone H3 (citH3) and neutrophil elastase (NE)-DNA complexes, both hallmarks of NETosis⁴⁰. Indeed, 6 h after stroke or myocardial infarction, we observed increased levels of citH3 and NE–DNA complexes in the blood (Fig. 5d, e and Extended data Fig. 5b). Interestingly, treatment of mice with DNase-I immediately after stroke reduced levels of citH3- and NE-DNA-complexes (Fig. 5d, e). To further validate the contribution of neutrophils to NET release and B cell loss in PP after stroke, we applied our established dual antibody-mediated depletion of circulating neutrophils (Extended data Fig. 5c)⁴¹. Indeed, neutrophil removal before the induction of stroke substantially reduced citH3 and NE-DNA complexes (Fig. 5d, e) and total ciDNA (Extended data Fig. 5d) and also completely inhibited the loss of B and T cells in PP (Fig. 5f and Extended data Fig. 5e), without affecting the brain infarct volumes (Extended data Fig. 5f). In addition, neutrophil depletion inhibited stroke-induced shrinkage of B cell follicles in PP (Extended data Fig. 5g). Acutely depleting neutrophils by antibody injection might have uncontrolled secondary effects on immune homeostasis. Hence, we generated mice, where neutrophils were absent due to the genetic removal of the critical survival factor Mcl⁴². Confirming our antibody-depletion experiments, the genetically induced loss of neutrophils in Ly6g^{cre}Mcl^{fl/fl} mice (Extended data Fig. 6a) showed significantly higher numbers of B cells in PP compared to neutrophil-sufficient Ly6g^{cre} mice 24 h after stroke (Fig. 5g) without changing the infarct volumes (Extended data Fig. 6b). Moreover, neutrophil-deficient Ly6g^{cre}Mcl^{fl/fl} mice also showed increased numbers of splenic T cells compared to stroke Ly6G^{cre} controls (Extended data Fig. 6c), thus suggesting the contribution of neutrophils in augmented ciDNA generation and T cell apoptosis-induction. In addition, when stroke mice were depleted of neutrophils, we not only found normalized levels of plasma IgA (Fig. 5h) but also a significant inhibition of PP shrinkage in all studied intestinal segments (Extended data Fig. 6d). Since we did only find small numbers of MPO⁺ neutrophils directly within the PP of stroke mice (Extended data Fig. 7a), we assume that acute NET production by circulating neutrophils in response to sterile injury is the major trigger that leads to PP lymphocyte cell death.

Next, we aimed to test the therapeutic targeting of NET formation for mucosal immune homeostasis during sterile tissue injury. First, stroke mice were treated with the pan PAD inhibitor Cl-amidine which has previously been shown to inhibit NET formation⁴³. Indeed, Cl-amidine treatment significantly reduced plasma levels of citH3-DNA complexes and prevented the loss of B cells in PP compared to vehicle-treated animals (Extended data Fig. 7b, c). However, Cl-amidine also reduced brain infarct sizes which indicated an additional neuroprotective effect of the compound (Extended data Fig. 7d). This, however, made it difficult

to dissect the impact of NETs or reduced brain-damage on B cell loss in PP. Therefore, we tested the Gasdermin D inhibitor LDC7559 to block NET formation after stroke⁴⁴. Interestingly, stroke mice treated with LDC7559 showed significantly reduced plasma levels of citH3 and NE-nucleosomes compared to the vehicle-treated group (Fig. 6a). Furthermore, the inhibition of NET formation, increased the numbers of IgD⁻ IgA⁺CD138⁻ plasma cell precursors (Fig. 6b) and mature IgD⁻ IgA⁺CD138⁺ plasma cells in PP and SI LP (Fig. 6c). In line with the increased numbers of plasma cells, we also found normalized levels of plasma IgA (Fig. 6d) and reduced shrinkage of B cell follicles in NET-inhibitor-treated stroke mice (Extended Data Fig. 7e). However, infarct volumes remained unchanged between treated and untreated groups (Extended Data Fig. 7f). These data show that post-injury activated neutrophils released toxic NETs which are responsible for the loss of functional B cells in PP and the reduced secretion of IgA.

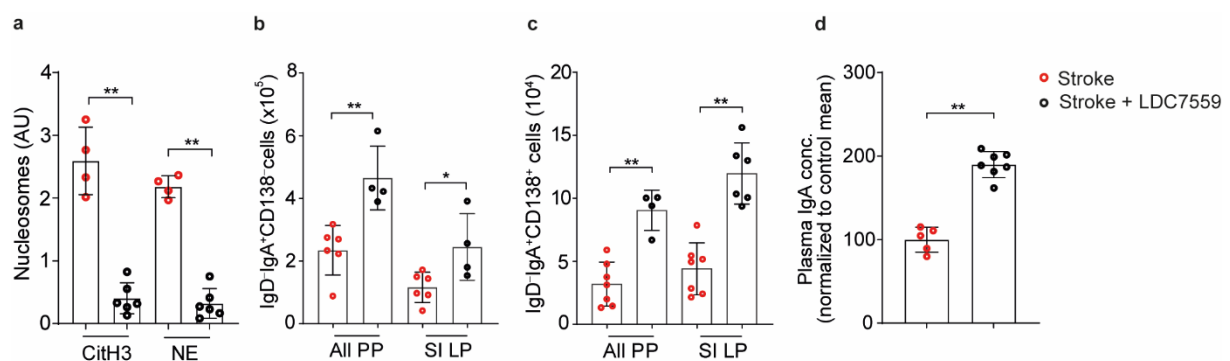


Fig. 6. Inhibition of NETs with a Gasdermin D blocker protects the number of IgA-secreting plasma cells after stroke. **a**, Relative plasma levels of citH3–DNA and NE–DNA complexes in stroke + vehicle and stroke + LDC7559 treated mice (n=4–6 per group). **b**, Numbers of IgA⁺ IgD⁻CD138⁻ plasma cell precursors in all PP and SI LP in stroke and stroke + LDC7559 treated mice. **c**, Numbers of IgA⁺ IgD⁻ CD138⁺ plasma cells in all PP and SI LP in stroke and stroke + LDC7559 treated mice. **d**, Relative concentrations of plasma IgA in stroke and stroke + LDC7559 treated mice. Data represent mean \pm s.d., two-tailed Mann–Whitney U test: *p<0.05, **p<0.01. All data is combined from at least two independent experiments, PP=Peyer’s patches, SI LP= small intestine lamina propria.

To evaluate the relevance of our experimental findings for the clinical reality, we finally analyzed circulating NETs in plasma samples of human ischemic stroke and myocardial infarct patients that were collected within 96 h of hospital admission. The blood samples from 9 equally aged healthy individuals were collected and processed with identical protocols. Our data confirmed, that the plasma of stroke patients contains significantly higher levels of citH3 and NE-DNA complexes compared to the healthy individuals (Fig. 7a, b) as seen elsewhere⁴⁵. Strikingly, the reduced levels of plasma IgA in stroke patients were highly significantly correlated with increasing amounts of circulating citH3-DNA complexes (Fig. 7c). Furthermore, the levels of citH3 and NE-DNA complexes were also significantly increased in the plasma of myocardial infarction patients compared to healthy subjects (Fig. 7d, e), thus suggesting NET-

release in human patients following the two most frequent causes of sterile tissue injury and death worldwide.

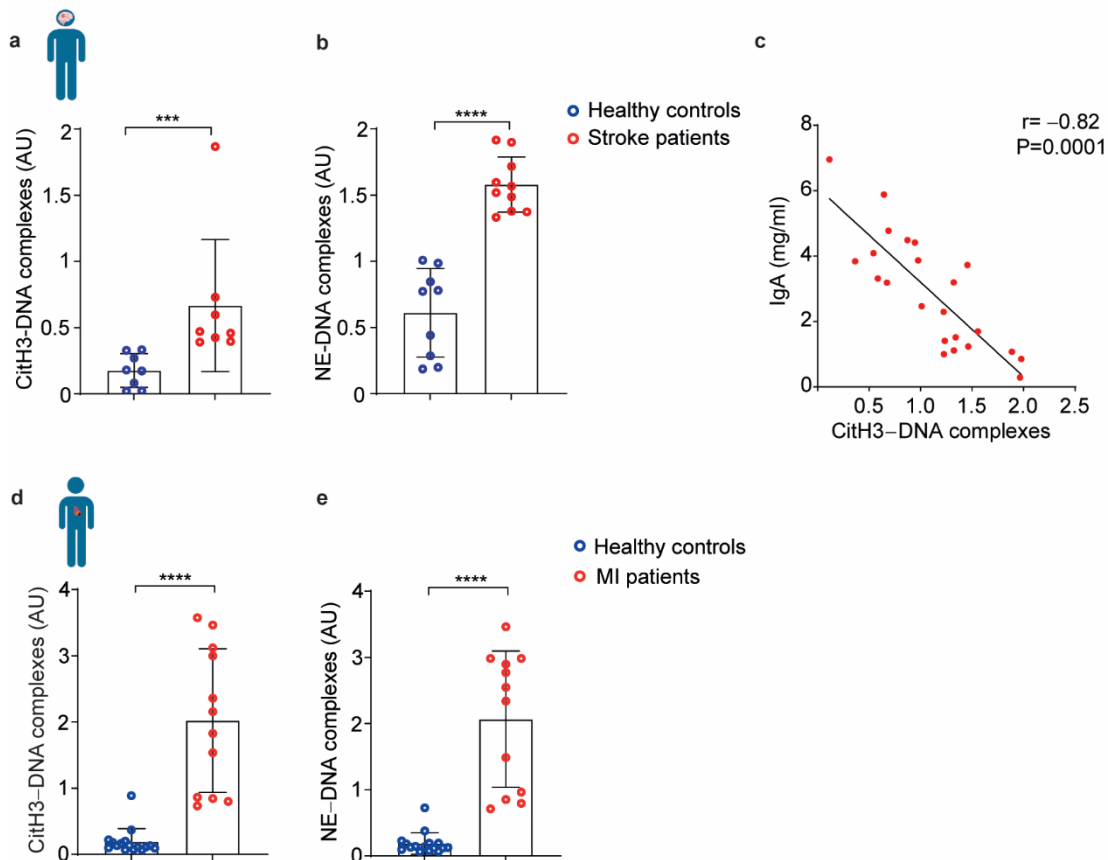


Fig. 7. Stroke and myocardial infarction patients show increased circulating NETs. **a**, Relative plasma levels of citH3–DNA and **b**, NE–DNA complexes in stroke patients and healthy subjects (n=8–10 per group). **c**, A highly significant negative correlation between plasma citH3–DNA complex levels and IgA amounts in stroke patients. **d**, Relative plasma levels of citH3–DNA and **e**, NE–DNA complexes in myocardial infarction patients and healthy controls (n=12–15 per group). Data represent mean \pm s.d., two-tailed Mann–Whitney U test: ***p<0.001, ****p<0.0001, MI= myocardial infarction, CitH3=citrullinated Histone-3, NE=neutrophil elastase.

Discussion

Here, we found that both, stroke and myocardial infarction, trigger lymphocyte death in intestinal mucosal tissues exposing an unexplored link between tissue injury and deteriorated intestinal immune function. The massive loss of lymphocytes and subsequent reduction in circulating and secretory IgA amounts were mediated via the release of toxic NETs from activated neutrophils after tissue injury.

Previous clinical studies have mentioned that reduced concentrations of IgA in stroke patients may increase susceptibility to bacterial infections⁸. In analogy, a recent clinical study reported higher mortality in myocardial infarction patients with concomitant bacterial infections⁴⁶. Within seven days of stroke onset, patients can show positive bacterial cultures in blood and urine¹.

Of note, more than 70% of detected bacteria in infected patients belong to human intestinal commensals, suggesting the translocation of bacteria through leaky intestinal mucosal barriers. Consequently, mature IgA-secreting plasma cells are key in protecting mucosal barriers. In addition, subsets of B cells can synthesize neurotrophins to support neuronal survival^{5,47}. The B-cell function on neuroregeneration after stroke⁴⁸ might be essential to counteract neuroinflammation induced by intestinal inflammatory T-cells^{49,50}. The effector functions of B cells are dependent on their survival, maintenance and differentiation and are transcriptionally tightly regulated⁵¹. Shortly after stroke, B cells in Peyer's patches (PP) upregulated proteins belonging to autophagy pathways representing the induction of chronic cellular stress. Moreover, the long-term effects of stroke on the reduction of B cells in intestinal PP are well supported by RNA sequencing data that revealed severe transcriptomic alterations in various apoptotic, survival and proliferation pathway genes of stroke mice^{32,33}.

Mechanistically, soluble mediators released after sterile tissue injury have been shown to activate neutrophils that then induce the formation of toxic NETs⁵². NETs consist of DNA, histones, and granular proteins and increase collateral inflammation and cell death. Recently, we showed that NETs directly induce smooth muscle cell death in arterial inflammation via attached histone-H4 proteins⁴². Our new proteomics results reveal now neutrophil activation as a consequence of tissue injury as early as six hours after an ischemic insult. Stroke increases the abundance of neutrophil activation-associated proteins such as S100A8, Lamp1 and Casp3 that might facilitate NET formation³⁹ as well as Aifm1, which is associated with chromatinolysis³⁷. Since neutrophil deficiency and NET blockade prevented the loss of IgA-producing intestinal immature and mature plasma cells after stroke, this study now provides a likely explanation for the previously unidentified source of ciDNA-inducing splenic T cell apoptosis¹⁷.

In recent years, DNase therapy has been largely proposed for the treatment of COVID-19⁵³ and psoriasis patients⁵⁴. Our findings that NETs are also present in the plasma of stroke and myocardial infarction patients would support clinical trials to test the efficacy of early DNase or NET inhibitor therapy to reduce immunosuppression and thereby improve disease outcomes. However, this would require that the focus of clinical stroke trials be expanded from evaluating neuroprotective outcomes alone to include immunoprotective effects, which could also have significant beneficial consequences for patients. With our identification of Gasdermin D as a novel target for specifically blocking NET release, further trials addressing this pathway are conceivable.

Collectively, our findings demonstrate that stroke and myocardial infarction lead to the immediate degeneration ("melting") of PP via the induction of NET release from hyper-activated neutrophils and the ensuing death of resident follicular B cells in mice. Although

previously speculated⁴⁵, this has not been experimentally proven until now. Massive NET release and the decline of intestinal lymphocytes appear to be a global response to sterile tissue necrosis. Previously, NETs have mainly been associated with impairment of post-stroke brain recovery⁵⁵. Here, we show substantial early effects on immune cell survival and function that open attractive treatment options by targeting NET-release or -function, for example as emergency therapy in patients with stroke or myocardial infarction.

Acknowledgments

This research work was funded by the Deutsche Forschungsgemeinschaft (DFG), research grant SI 2650/1-1 to VS, GU 769/10-1 to MGU, HE3173/11-1, 3173/12-1, 3173/13-1 and 3173/15-1 to DMH, RA969/12-1 to TR and the CRC TRR332 (project C6) to MGU and DMH, project A2 to OS and project C5 to AG. The work of SS and JC was supported by the Bundesministerium für Bildung und Forschung, BMBF, Ref. 161L0272. The work of ISAS was supported by the “Ministerium für Kultur und Wissenschaft des Landes Nordrhein-Westfalen” and “Der Regierende Bürgermeister von Berlin, Senatskanzlei Wissenschaft und Forschung.” The microscopy and flow cytometry work in this manuscript was performed at the Imaging Center Essen (IMCES) a service core facility of the faculty of medicine of the University Duisburg-Essen, Germany. We thank Alexandra Brenzel and Anthony Squire at IMCES for their technical support. We thank Ari Waisman and Michaela Blanford for providing the intestinal tracts of Igh-J mice. Axel Choidas and Bert Klebl from LDC are acknowledged for help with LDC7559 experiments. We thank Adrian Moenig and Andreas Giese for their help with patient sample collection. All authors have read and approved the manuscript, and the manuscript has not been accepted or published elsewhere.

Author contributions

AAT, SG, MGa, DT, SPS, AK, ÖU, FZ, VK, VL, AQ, ZC, MA, SK, LM, TR, BK, HA, AMY, CW, LH, SL, NH, AH, JC, and VS performed experiments and analyzed the data. MS, OS, BF, MK, JS, MT, DH, AG, AS, DMH, contributed essential materials and in-depth discussion of the results. AAT, MGU and VS wrote the manuscript and all authors revised the manuscript and approved its final version. MGU. and VS conceived and supervised the project.

Declaration of interests

The authors declare no competing financial interests.

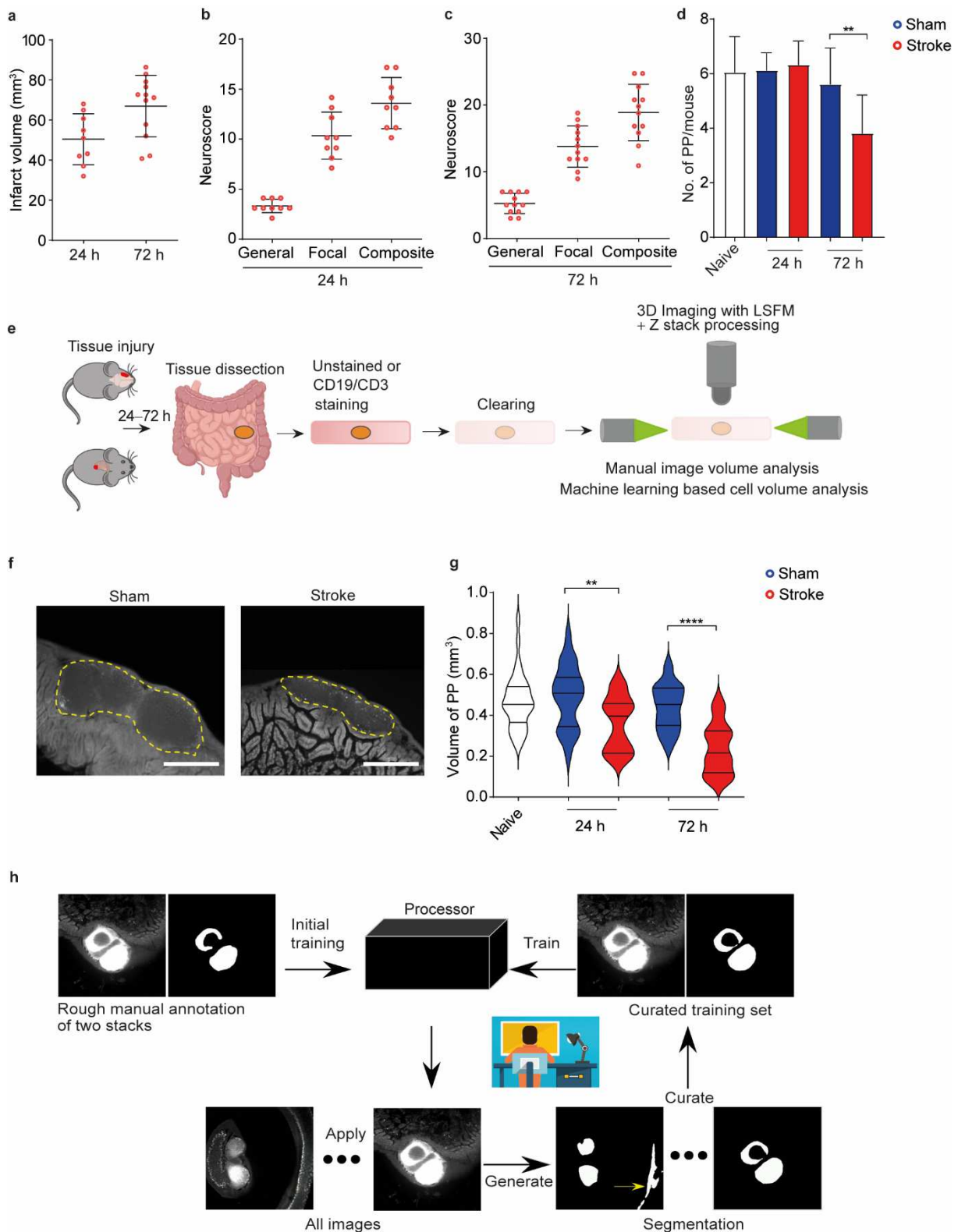
References

1. Stanley, D. *et al.* Translocation and dissemination of commensal bacteria in post-stroke infection. *Nat Med* **22**, 1277-1284 (2016).
2. Liu, Y. *et al.* Risk Estimation for Infection in Patients With ST-Segment Elevation Myocardial Infarction Undergoing Percutaneous Coronary Intervention: Development and Validation of a Predictive Score. *Front Cardiovasc Med* **9**, 845307 (2022).
3. Putot, A., Chague, F., Manckoundia, P., Cottin, Y. & Zeller, M. Post-Infectious Myocardial Infarction: New Insights for Improved Screening. *J Clin Med* **8** (2019).
4. Lycke, N.Y. & Bemark, M. The regulation of gut mucosal IgA B-cell responses: recent developments. *Mucosal Immunol* **10**, 1361-1374 (2017).
5. Kombar, R.J. *et al.* Activated Peyer's patch B cells sample antigen directly from M cells in the subepithelial dome. *Nat Commun* **10**, 2423 (2019).
6. Lin, S. *et al.* Mucosal immunity-mediated modulation of the gut microbiome by oral delivery of probiotics into Peyer's patches. *Sci Adv* **7** (2021).
7. Shirakashi, M. *et al.* Effect of Impaired T Cell Receptor Signaling on the Gut Microbiota in a Mouse Model of Systemic Autoimmunity. *Arthritis Rheumatol* **74**, 641-653 (2022).
8. McCulloch, L., Allan, S.M., Emsley, H.C., Smith, C.J. & McColl, B.W. Interleukin-1 receptor antagonist treatment in acute ischaemic stroke does not alter systemic markers of anti-microbial defence. *F1000Res* **8**, 1039 (2019).
9. Iadecola, C. & Anrather, J. The immunology of stroke: from mechanisms to translation. *Nat Med* **17**, 796-808 (2011).
10. Learoyd, A.E. *et al.* Infections Up to 76 Days After Stroke Increase Disability and Death. *Transl Stroke Res* **8**, 541-548 (2017).
11. Zundler, S. *et al.* Three-Dimensional Cross-Sectional Light-Sheet Microscopy Imaging of the Inflamed Mouse Gut. *Gastroenterology* **153**, 898-900 (2017).
12. Schleier, L. *et al.* Non-classical monocyte homing to the gut via alpha4beta7 integrin mediates macrophage-dependent intestinal wound healing. *Gut* **69**, 252-263 (2020).
13. Offner, H. *et al.* Splenic atrophy in experimental stroke is accompanied by increased regulatory T cells and circulating macrophages. *J Immunol* **176**, 6523-6531 (2006).
14. Merz, S.F. *et al.* Contemporaneous 3D characterization of acute and chronic myocardial I/R injury and response. *Nat Commun* **10**, 2312 (2019).
15. Michel, L. *et al.* Targeting early stages of cardiotoxicity from anti-PD1 immune checkpoint inhibitor therapy. *Eur Heart J* (2021).
16. Gu, H., Zou, Y.R. & Rajewsky, K. Independent control of immunoglobulin switch recombination at individual switch regions evidenced through Cre-loxP-mediated gene targeting. *Cell* **73**, 1155-1164 (1993).
17. Roth, S. *et al.* Post-injury immunosuppression and secondary infections are caused by an AIM2 inflammasome-driven signaling cascade. *Immunity* **54**, 648-659 e648 (2021).
18. Singh, V. *et al.* Stroke increases the expression of ACE2, the SARS-CoV-2 binding receptor, in murine lungs. *Brain Behav Immun* **94**, 458-462 (2021).
19. Trindade, B.C. *et al.* The cholesterol metabolite 25-hydroxycholesterol restrains the transcriptional regulator SREBP2 and limits intestinal IgA plasma cell differentiation. *Immunity* **54**, 2273-2287 e2276 (2021).
20. Lecuyer, E. *et al.* Segmented filamentous bacterium uses secondary and tertiary lymphoid tissues to induce gut IgA and specific T helper 17 cell responses. *Immunity* **40**, 608-620 (2014).
21. Reboldi, A. *et al.* IgA production requires B cell interaction with subepithelial dendritic cells in Peyer's patches. *Science* **352**, aaf4822 (2016).

22. Clancy-Thompson, E. *et al.* Transnuclear mice reveal Peyer's patch iNKT cells that regulate B-cell class switching to IgG1. *EMBO J* **38**, e101260 (2019).
23. Li, L., Gao, L., Song, Y., Qin, Z.H. & Liang, Z. Activated cathepsin L is associated with the switch from autophagy to apoptotic death of SH-SY5Y cells exposed to 6-hydroxydopamine. *Biochem Biophys Res Commun* **470**, 579-585 (2016).
24. Huynh, K.K. *et al.* LAMP proteins are required for fusion of lysosomes with phagosomes. *EMBO J* **26**, 313-324 (2007).
25. Carilla-Latorre, S., Annesley, S.J., Munoz-Braceras, S., Fisher, P.R. & Escalante, R. Ndufa5 deficiency in the Dictyostelium model: new roles in autophagy and development. *Mol Biol Cell* **24**, 1519-1528 (2013).
26. Salvi, A. *et al.* PHY34 inhibits autophagy through V-ATPase V0A2 subunit inhibition and CAS/CSE1L nuclear cargo trafficking in high grade serous ovarian cancer. *Cell Death Dis* **13**, 45 (2022).
27. Rizvi, F. *et al.* Effects of Aging on Cardiac Oxidative Stress and Transcriptional Changes in Pathways of Reactive Oxygen Species Generation and Clearance. *J Am Heart Assoc* **10**, e019948 (2021).
28. Shi, X. *et al.* ndufa7 plays a critical role in cardiac hypertrophy. *J Cell Mol Med* **24**, 13151-13162 (2020).
29. Liu, Y. *et al.* Autosis is a Na⁺,K⁺-ATPase-regulated form of cell death triggered by autophagy-inducing peptides, starvation, and hypoxia-ischemia. *Proc Natl Acad Sci U S A* **110**, 20364-20371 (2013).
30. Woess, C. *et al.* Combined loss of the BH3-only proteins Bim and Bmf restores B-cell development and function in TACI-Ig transgenic mice. *Cell Death Differ* **22**, 1477-1488 (2015).
31. Taylor, J. *et al.* B-cell receptor signaling induces proteasomal degradation of PDCD4 via MEK1/2 and mTORC1 in malignant B cells. *Cell Signal* **94**, 110311 (2022).
32. Ramezani-Rad, P., Chen, C., Zhu, Z. & Rickert, R.C. Cyclin D3 Governs Clonal Expansion of Dark Zone Germinal Center B Cells. *Cell Rep* **33**, 108403 (2020).
33. Kurschat, C., Metz, A., Kirschnek, S. & Hacker, G. Importance of Bcl-2-family proteins in murine hematopoietic progenitor and early B cells. *Cell Death Dis* **12**, 784 (2021).
34. Emily Robinson, M.C., Reuben Tooze and Gina Doody. Salt-Inducible kinases are critical regulators of terminal B-cell differentiation. *J Immunol* **200**, 171.173 (2018).
35. Dai, X. *et al.* A disease-associated PTPN22 variant promotes systemic autoimmunity in murine models. *J Clin Invest* **123**, 2024-2036 (2013).
36. Brinkmann, V. *et al.* Neutrophil extracellular traps kill bacteria. *Science* **303**, 1532-1535 (2004).
37. Tang, D., Kang, R., Berghe, T.V., Vandenabeele, P. & Kroemer, G. The molecular machinery of regulated cell death. *Cell Res* **29**, 347-364 (2019).
38. Vorobjeva, N.V. & Chernyak, B.V. NETosis: Molecular Mechanisms, Role in Physiology and Pathology. *Biochemistry (Mosc)* **85**, 1178-1190 (2020).
39. Sprenkeler, E.G.G. *et al.* S100A8/A9 Is a Marker for the Release of Neutrophil Extracellular Traps and Induces Neutrophil Activation. *Cells* **11** (2022).
40. Tsourouktsoglou, T.D. *et al.* Histones, DNA, and Citrullination Promote Neutrophil Extracellular Trap Inflammation by Regulating the Localization and Activation of TLR4. *Cell Rep* **31**, 107602 (2020).
41. Boivin, G. *et al.* Durable and controlled depletion of neutrophils in mice. *Nat Commun* **11**, 2762 (2020).
42. Silvestre-Roig, C. *et al.* Externalized histone H4 orchestrates chronic inflammation by inducing lytic cell death. *Nature* **569**, 236-240 (2019).
43. Thiam, H.R. *et al.* NETosis proceeds by cytoskeleton and endomembrane disassembly and PAD4-mediated chromatin decondensation and nuclear envelope rupture. *Proc Natl Acad Sci U S A* **117**, 7326-7337 (2020).
44. Sollberger, G. *et al.* Gasdermin D plays a vital role in the generation of neutrophil extracellular traps. *Sci Immunol* **3** (2018).

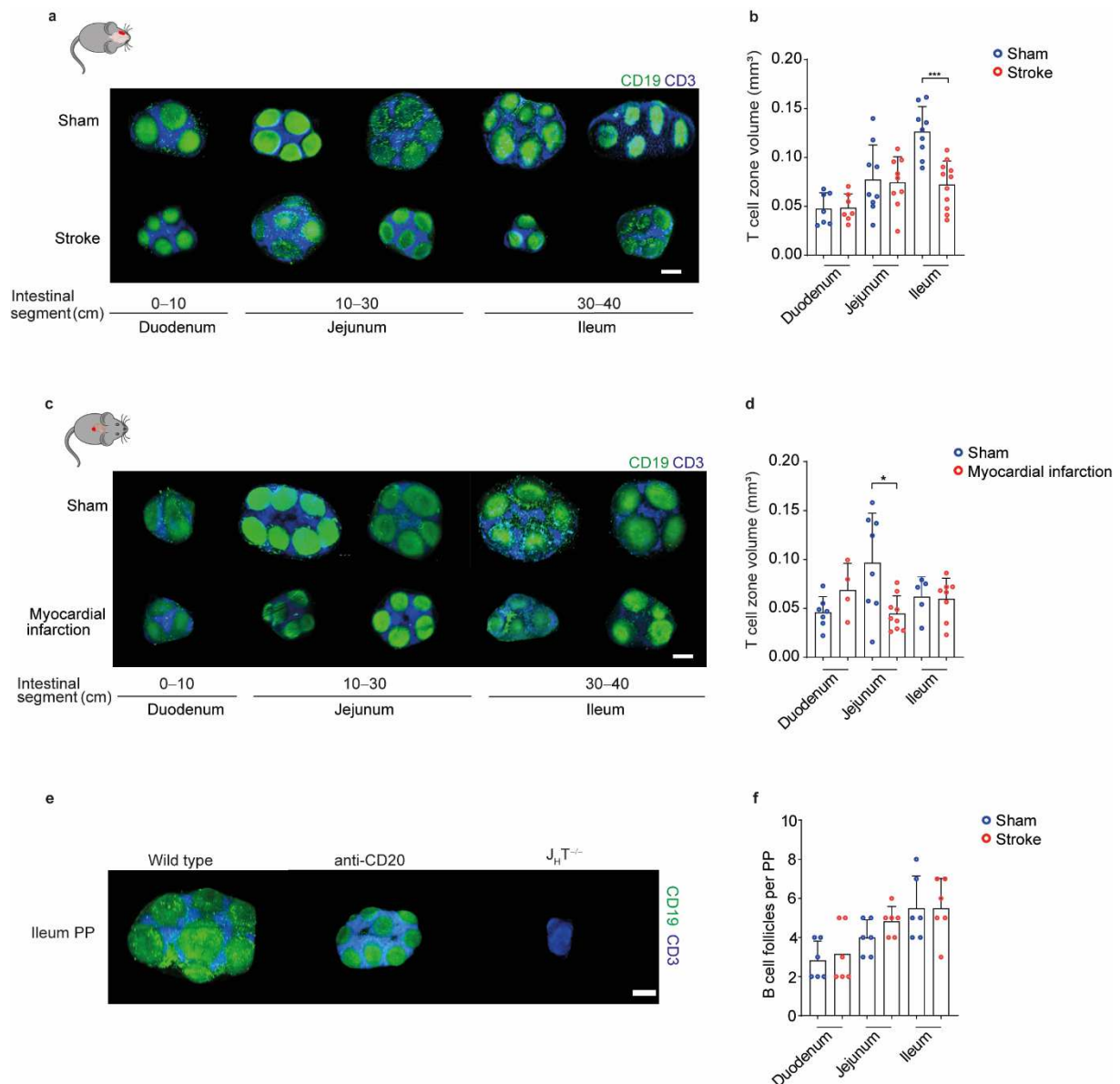
45. Grosse, G.M. *et al.* Endogenous Deoxyribonuclease Activity and Cell-Free Deoxyribonucleic Acid in Acute Ischemic Stroke: A Cohort Study. *Stroke* **53**, 1235-1244 (2022).
46. Qian L , Z.S., Lin J , Li Z. In-Hospital Outcomes and Biomarkers of Acute Myocardial Infarction With Concomitant Bacterial infection : A Retrospective Study. *Preprint from Research Square*, (2022).
47. Ren, X. *et al.* Regulatory B cells limit CNS inflammation and neurologic deficits in murine experimental stroke. *J Neurosci* **31**, 8556-8563 (2011).
48. Ortega, S.B. *et al.* B cells migrate into remote brain areas and support neurogenesis and functional recovery after focal stroke in mice. *Proc Natl Acad Sci U S A* **117**, 4983-4993 (2020).
49. Singh, V. *et al.* Microbiota Dysbiosis Controls the Neuroinflammatory Response after Stroke. *J Neurosci* **36**, 7428-7440 (2016).
50. Benakis, C. *et al.* Commensal microbiota affects ischemic stroke outcome by regulating intestinal gammadelta T cells. *Nat Med* **22**, 516-523 (2016).
51. Laidlaw, B.J. & Cyster, J.G. Transcriptional regulation of memory B cell differentiation. *Nat Rev Immunol* **21**, 209-220 (2021).
52. Mulay, S.R. & Anders, H.J. Neutrophils and Neutrophil Extracellular Traps Regulate Immune Responses in Health and Disease. *Cells* **9** (2020).
53. Fisher, J. *et al.* Proteome Profiling of Recombinant DNase Therapy in Reducing NETs and Aiding Recovery in COVID-19 Patients. *Mol Cell Proteomics* **20**, 100113 (2021).
54. Shao, S. *et al.* Neutrophil Extracellular Traps Promote Inflammatory Responses in Psoriasis via Activating Epidermal TLR4/IL-36R Crosstalk. *Front Immunol* **10**, 746 (2019).
55. Kang, L. *et al.* Neutrophil extracellular traps released by neutrophils impair revascularization and vascular remodeling after stroke. *Nat Commun* **11**, 2488 (2020).

Supplementary data



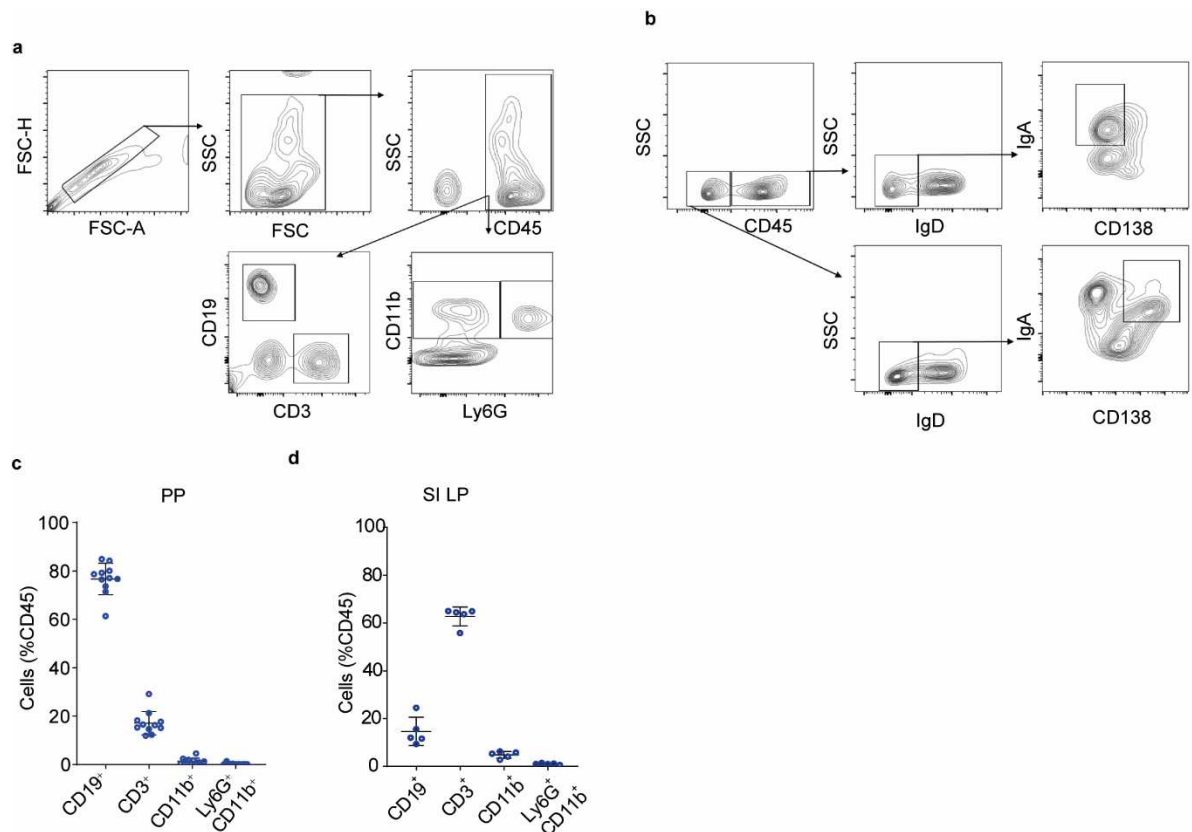
Extended Data Fig. 1. Stroke induces sensorimotor deficits and its impact on PP B cell follicles volume is analyzed using LSFM. **a**, Quantification of brain infarct volume after 24 h and 72 h of stroke (n=9–12 per group). **b**, Neurological deficits are measured at 24 h and **c**, 72 h after stroke (n=9–12 per group). **d**, The total number of intestinal PP per mouse 24 h and 72 h after sham surgery or stroke or unoperated naïve mice (n=8–13 mice per group). **e**, Illustration of the intestinal tissue preparation for unstained–volume analysis of whole PP or whole–mount

staining of B and T cells in PP, followed by tissue clearing and LSFM-based 3D volume analysis. **f**, Representative LSFM images of cleared unstained intestinal PP showing their shrinkage 24 h after sham or stroke, scale bar=500 μm . **g**, Tissue volume analysis of PP after 24 h and 72 h of sham or stroke; (n=23 PP for sham and n=16 PP for stroke, n=3–4 mice for 24 h and n=34 PP for sham and n=24 PP for stroke, n=6 mice for 72 h). **h**, Overview of the human-in-the-loop segmentation workflow for automated analysis of B cell follicles volume and T cell zone volume. Data represented as mean \pm s.d., statistical analyses were performed by two-tailed Mann-Whitney U test, $**p < 0.01$, All data are combined from at least three independent experiments. PP=Peyer's patches.

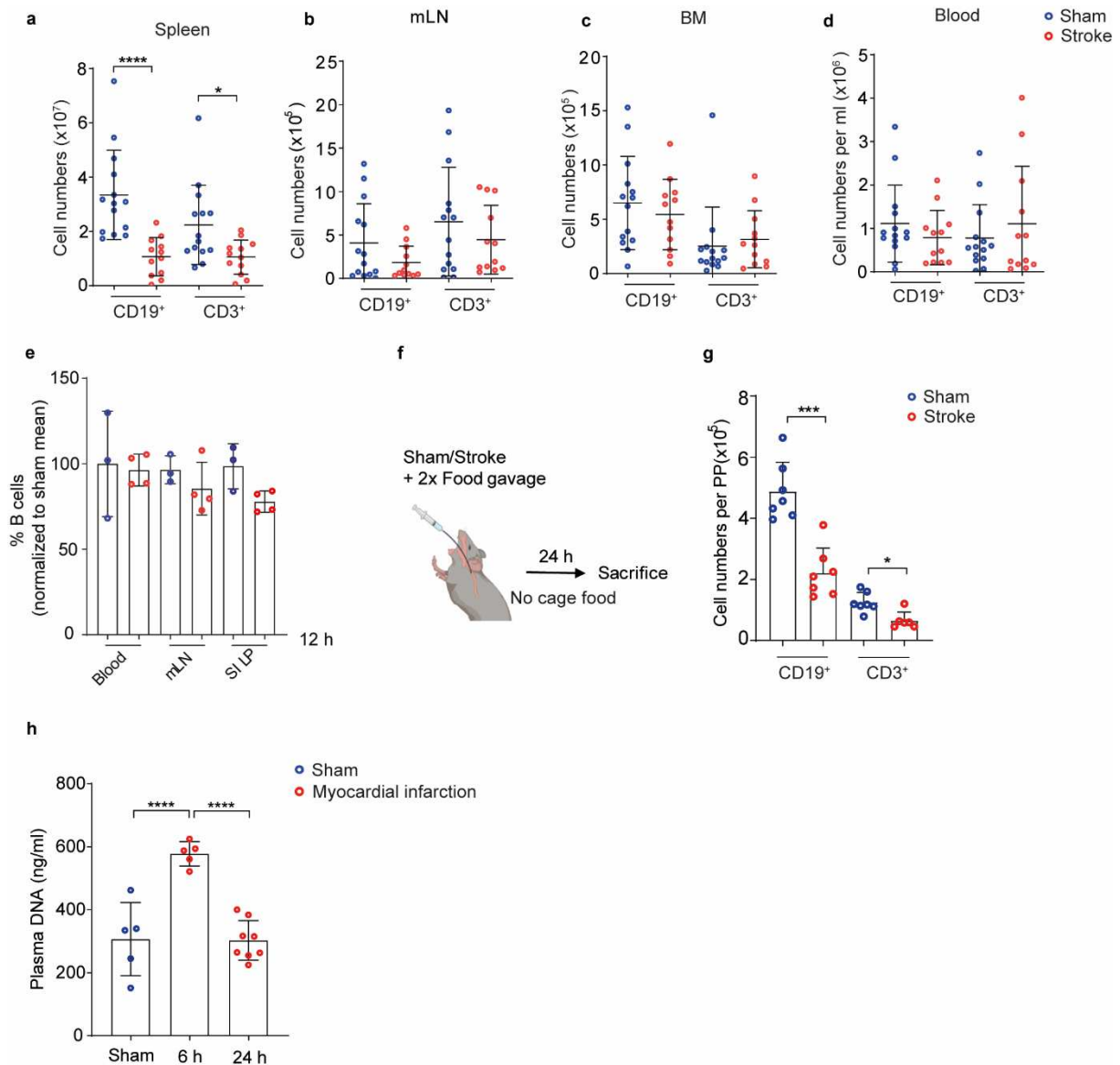


Extended Data Fig. 2. Stroke and myocardial infarction induces shrinkage of B cell follicles and T cell zone volumes in PP. **a**, 3D reconstruction images of CD19⁺ B cells and CD3⁺ T cells in PP isolated from duodenum, jejunum and ileum 24 h after stroke or sham surgery, scale bar=500 μm . **b**, The quantification of T cell zone volume in different intestinal segments after 24 h of stroke or sham controls (n=8-11 PP per intestinal segment). **c**, 3D reconstruction images of CD19⁺ B cells and CD3⁺ T cells in PP isolated from duodenum, jejunum and ileum 24 h after myocardial infarction or sham surgery. **d**, The quantification of T cell zone volume in different intestinal

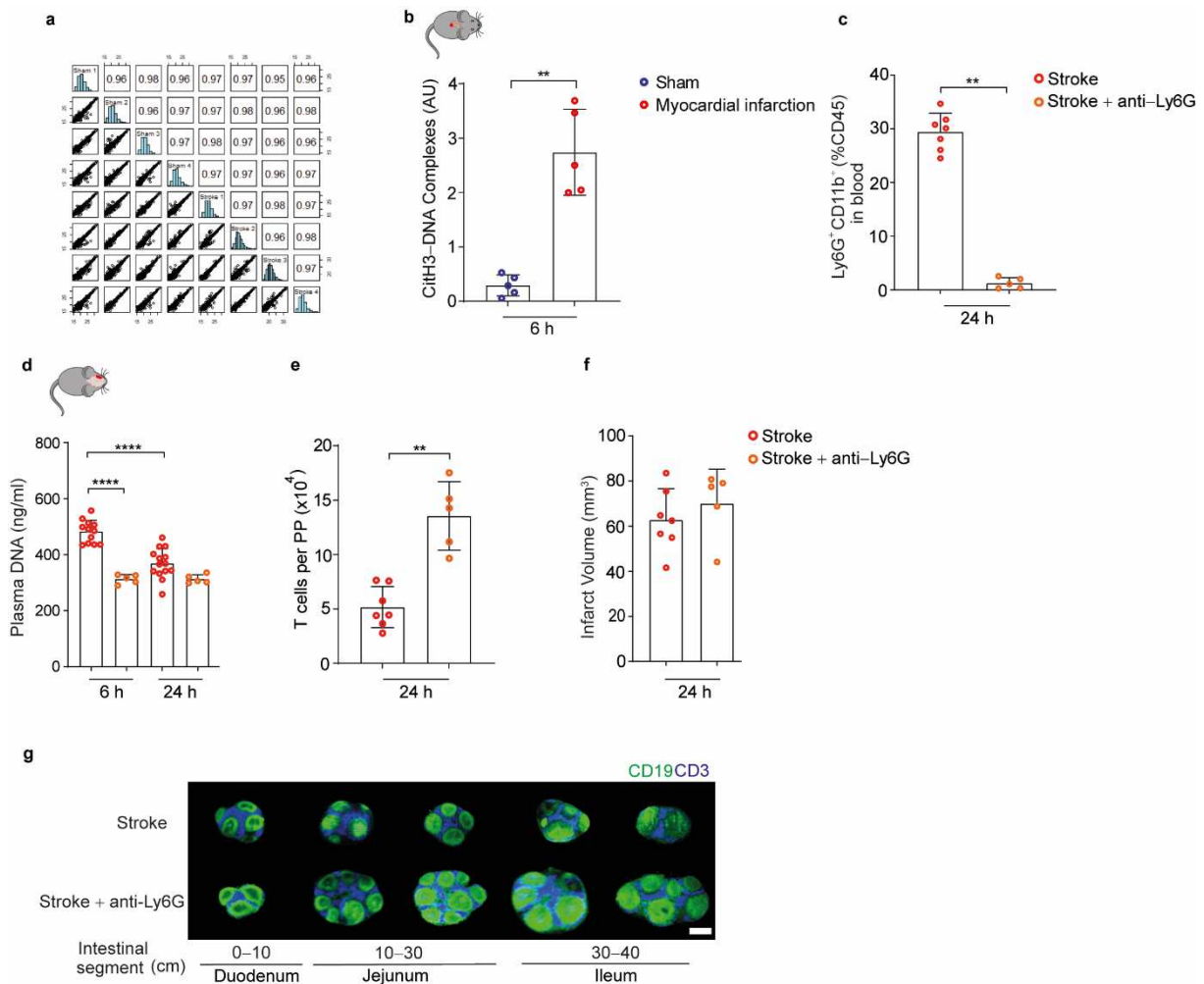
segments after 24 h of myocardial infarction or sham controls (n=4–6 PP per intestinal segment). **e**, 3D reconstruction images of CD19⁺ B cells and CD3⁺ T cells in PP isolated from ileum of naïve Wild type, anti-CD20 treated wild type and J_hT^{-/-} mice. **f**, Quantification of the number of B cell follicles per PP in different intestinal regions after stroke or sham operation. Data represented as mean ±s.d., statistical analyses were performed by two-tailed Mann–Whitney U test, *p<0.05, ***p<0.001. All data are combined from at least three independent experiments. PP=Peyer’s patches.



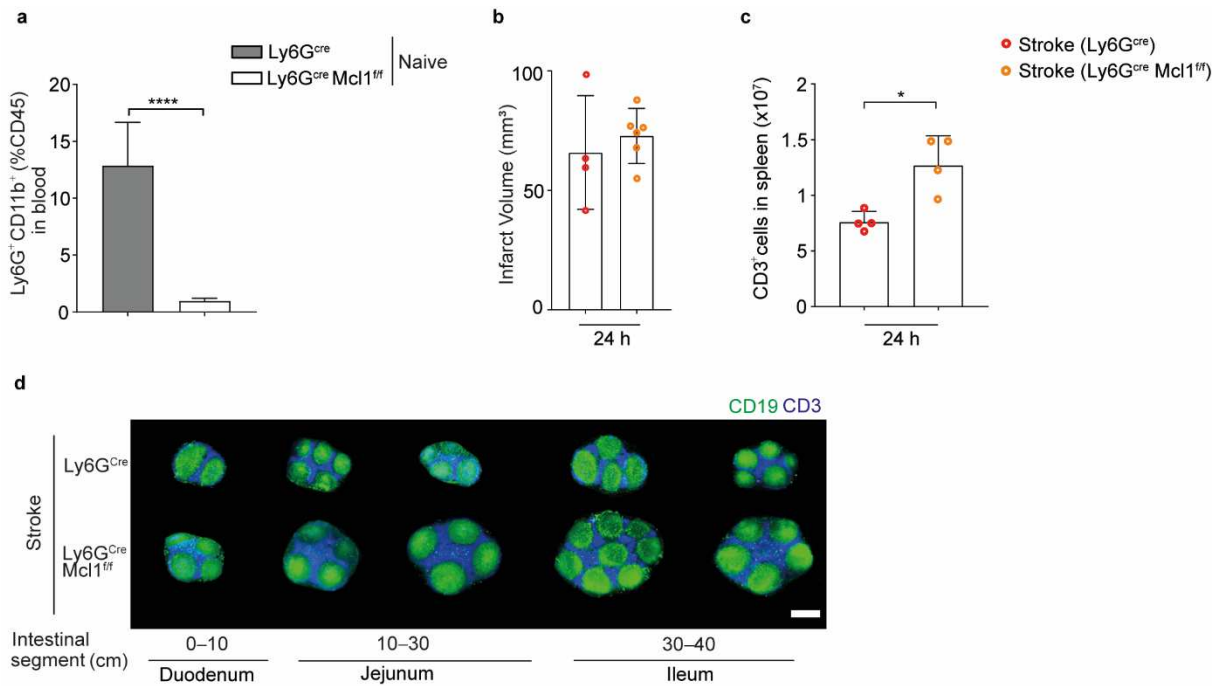
Extended Data Fig. 3. Differential frequencies of B and T cells in Peyer’s patches and small intestine lamina propria. **a**, Representative gating strategy for the analysis of lymphocytes and granulocytes using multi-color flow cytometry. **b**, Representative gating strategy for the analysis of class-switched IgA-producing precursors and mature plasma cell subsets using multi-color flow cytometry. **c,d** The frequency of CD19⁺, CD3⁺, CD11b⁺ and Ly6G⁺ CD11b⁺ cells in PP and SI LP of sham mice. Data represented as mean ±s.d..All data are combined from at least three independent experiments. PP=Peyer’s patches, SI LP=small intestine lamina propria.



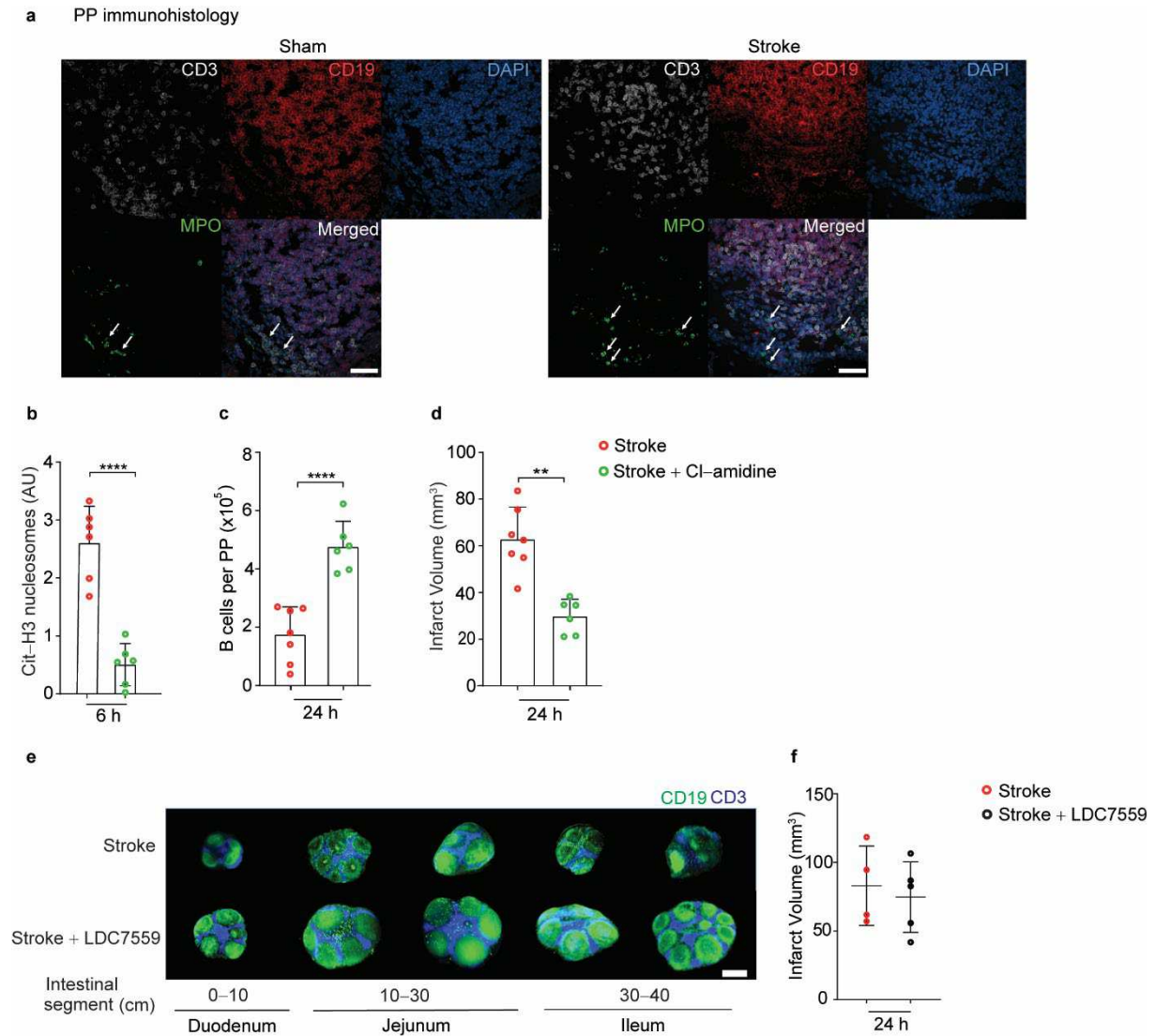
Extended Data Fig. 4. Stroke differentially impacts lymphocyte numbers in lymphoid tissues and is independent of reduced food consumption. **a**, Total numbers of CD19⁺ B cells and CD3⁺ T cells in spleens of stroke or sham-operated mice (n=12–14 per group). **b-d**, Total numbers of CD19⁺ B cells and CD3⁺ T cells in mLN, BM and blood of stroke or sham-operated mice (n=12–14 per group). **e**, Relative frequencies of B cells in blood, mLN and SI LP after 12 h of stroke or sham-operation (n=3–4 per group) normalized to mean of sham. **f**, Mice underwent stroke or sham surgery and received two times food gavage and were sacrificed 24 h after the operation to analyze the number of B and T cells in PP. **g**, Total numbers of CD19⁺ B cells and CD3⁺ T cells in PP of stroke or sham-operated mice that received food gavage (n=7 per group). **h**, Quantification of plasma DNA content in sham-operated or myocardial infarction mice. Data represented as mean \pm s.d., Shapiro-Wilk normality, and ordinary one-way ANOVA with Bonferroni's multiple comparisons tests and for comparisons between two groups two-tailed Mann-Whitney U test, *p<0.05, ***p<0.001, ****p<0.0001. PP=Peyer's patches, SI LP=small intestine lamina propria, mLN=mesenteric lymph nodes.



Extended Data Fig. 5. Neutrophil-released NETs after tissue injury contributes to reduced B and T cell numbers in PP. **a**, A sample-wise comparison showed a Pearson correlation coefficient for all analyzed samples for mass spectrometry analysis. **b**, Relative plasma levels of citH3-DNA complexes after 6 h of myocardial infarction or sham operation (n=5 per group). **c**, Relative frequencies of blood Ly6G⁺CD11b⁺ neutrophils in stroke mice treated with anti-ly6G antibodies or vehicle (n=5-7 per group). **d**, Quantification of plasma DNA at 6 h and 24 h after stroke + isotype antibody or stroke + anti-Ly6G antibody injected mice (n=5-14 per group). **e**, The total numbers of CD3⁺ T cells in PP of stroke + isotype antibody or stroke + anti-Ly6G antibody-injected mice after 24 h (n=5-6 per group). **f**, Brain infarct volumes after 24 h of stroke + isotype antibody or stroke + anti-Ly6G antibody-injected mice (n=5-7 per group). **g**, 3D reconstruction images of CD19⁺ B cells and CD3⁺ T cells in PP isolated from duodenum, jejunum and ileum 24 h of stroke + isotype antibody or stroke + anti-Ly6G treated mice, scale bar=500 μ m. Data represented as mean \pm s.d., Shapiro-Wilk normality, and ordinary one-way ANOVA with Bonferroni's multiple comparisons tests and for comparisons between two groups two-tailed Mann-Whitney U test, **p<0.01, ****p<0.0001. PP=Peyer's patch, CitH3=citrullinated Histone-3.



Extended Data Fig. 6. Neutrophil-deficiency blocked stroke triggered lymphocyte loss and shrinkage of B cell follicles in PP. **a**, Percentages of blood Ly6G⁺ CD11b⁺ neutrophils in naïve Ly6G^{cre} and Ly6G^{cre}Mcl1^{ff} mice (n=11–15 per group). **b**, Brain infarct volumes after 24 h of stroke in Ly6G^{cre} and Ly6G^{cre}Mcl1^{ff} mice (n=4–6 per group). **c**, Total numbers of CD3⁺ T cells after 24 h of stroke in spleens of Ly6G^{cre} and Ly6G^{cre}Mcl1^{ff} mice (n=4 per group). **d**, 3D reconstruction images of CD19⁺ B cells and CD3⁺ T cells in PP isolated from duodenum, jejunum and ileum 24 h after stroke in Ly6G^{cre} and Ly6G^{cre}Mcl1^{ff} mice, scale bar=500 μ m. Data represented as mean \pm s.d., statistical analyses were performed by two-tailed Mann-Whitney U test, *p<0.05, ****p<0.0001.



Extended Data Fig. 7. Pharmacological inhibition of NET formation blocked stroke triggered lymphocyte loss and reduction of B cell follicles in PP. **a**, Representative fluorescence histology images of PP stained with, anti-CD3, anti-CD19, anti-MPO and DAPI after 12 h of stroke and sham operation, scale bar=20 μ m. **b**, Relative plasma levels of citH3-DNA complexes after 6 h of stroke or Bi + Cl-amidine treated mice (n=6 per group). **c**, Total numbers of B cells in PP of stroke + vehicle or stroke + Cl-amidine treated mice after 24 h (n=6-7 mice per group). **d**, Brain infarct volumes after 24 h of stroke + vehicle or stroke + Cl-amidine treated mice (n=6-7 per group). **e**, 3D reconstruction images of CD19⁺ B cells and CD3⁺ T cells in PP isolated from duodenum, jejunum and ileum 24 h of stroke + vehicle or stroke + LDC7559 treated mice, scale bar=500 μ m. **f**, Brain infarct volumes after 24 h of stroke + vehicle or stroke + LDC7559 treated mice (n=4-6 per group). Data represented as mean \pm s.d., statistical analyses were performed by two-tailed Mann-Whitney U test, **p<0.01, ****p<0.0001. PP=Peyer's patches.

Supplementary Files

This is a list of supplementary files associated with this preprint. Click to download.

- [MaterialsandMethodsSingh.pdf](#)
- [SupplementaryVideoText.pdf](#)
- [Video1CellulararchitectureofPP.avi](#)
- [Video2PPaftershamandStroke.avi](#)